Brain Research Bulletin 183 (2022) 57–72

Contents lists available at ScienceDirect

Brain Research Bulletin

journal homepage: www.elsevier.com/locate/brainresbull

The effect of astaxanthin treatment on the rat model of fetal alcohol spectrum disorders (FASD)

Mu-Hsuan Chen [a], Cih-Li Hong [b], Yi-Ting Wang [b], Tsyr-Jiuan Wang [c,*], Jeng-Rung Chen [a,b,**]

[a] Program in Tissue Engineering and Regenerative Medicine, National Chung-Hsing University, Taichung, Taiwan
[b] Department of Veterinary Medicine, College of Veterinary Medicine, National Chung-Hsing University, Taichung, Taiwan
[c] Department of Nursing, National Taichung University of Science and Technology, Taichung, Taiwan

ARTICLE INFO

Keywords:
Fetal alcohol spectrum disorders
Astaxanthin
Neuroinflammation
Oxidative stress
Cholinergic neurons
Dendritic spine
Hippocampus
Cognitive function

ABSTRACT

Fetal alcohol spectrum disorder (FASD) caused by mother's exposure to alcohol during pregnancy is a congenital neurological disease of the fetus resulting in fetal developmental and intellectual disabilities, cognitive impairment, and coordination disorder. Excess oxidative stress and neuroinflammatory responses were an important factor in neuropathological changes in FASD. Astaxanthin (AST) was a potent antioxidant and anti-inflammatory carotenoid. Therefore, this study proposed to explore how AST treatment can ameliorate morphological changes in the hippocampus and cognitive impairment in FASD rats by reducing oxidative stress and neuroinflammation in the brain. An alcohol atomizer was used from postnatal day (P) 2 to P10 to induce the FASD rat model. They were treated with AST (10 mg/kg body weight/day, intraperitoneal injection) for 8 consecutive days starting at P53 and sacrificed at P60. FASD rats had growth retardation and facial dysmorphologies, excessive oxidative stress and neuroinflammation in the hippocampus, decreased choline acetyltransferase (ChAT) expression in MS nucleus, spine loss on hippocampal CA1 pyramidal neurons, and poor performance in spatial learning and memory and sensory-motor coordination. After AST treatment, oxidative stress, neuroinflammation, cholinergic system, excitatory synaptic structure and behavior of FASD rats improved. Therefore, our study provided evidence to support the proposal that AST could be considered to treat FASD.

1. Introduction

FASD is a birth defect that is caused by the mother with alcohol consumption during pregnancy and displays physical, mental, behavioral, and learning disabilities with lifelong implications. It is a spectrum that describes the range of effects of maternal exposure to ethanol, including fetal alcohol syndrome (FAS), partial fetal alcohol syndrome (pFAS), alcohol-related neurobehavioral disorder (ARND), neurobehavioral disorder associated with prenatal alcohol exposure (ND-PAE), and alcohol-related birth defects (ARBD). There were many common characteristics among people who suffered from the effects of alcohol exposure, such as abnormal facial features, smaller head size, stunted growth, behavioral abnormalities, and learning disabilities (Wattendorf and Muenke, 2005). Apart from the above, structural changes in the human brain were also observed, including permanent loss of tissue in the corpus callosum, damage to the basal ganglia, and stunted growth of the cerebellum (Norman et al., 2009). Animal studies provide some insight that the severity of FASD is influenced by multiple factors, including the timing, amount, or pattern of fetal exposure to alcohol. The morphology and function of embryonic development have

Abbreviations: AST, astaxanthin; BAC, blood alcohol concentration; BBB, blood-brain barrier; BDNF, brain-derived neurotrophic factor; BWT, beam walking test; CAT, catalase; ChAT, choline acetyltransferase; CNS, central nervous system; COX, cyclooxygenase; DAPI, 4',6-diamidino-2-phenylindole; ELISA, enzyme-linked immunosorbent assay; FASD, fetal alcohol spectrum disorder; GFAP, glial fibrillary acidic protein; GPx, glutathione peroxidase; H_2O_2, hydrogen peroxide; Iba1, ionized calcium binding adaptor molecule 1; IL, interleukin; iNOS, inducible nitric oxide synthase; LY, Lucifer yellow; MDA, malondialdehyde; MS, medial septal; MWM, Morris water maze; NADH, nicotinamide adenine dinucleotide; NF-κB, nuclear factor kappa-light-chain-enhancer of activated B cells; NGF, nerve growth factor; nNOS, neuronal nitric oxide synthase; NO, nitric oxide; Nrf2, nuclear factor erythroid-related factor 2; P, postnatal day; PB, phosphate buffer; PBS, phosphate-buffer saline; PFA, paraformaldehyde; PI3K, phosphoinositide 3-kinase; ROS, reactive oxygen species; SOD, dismutase; TBARS, thiobarbituric acid reactive substance; TNF-α, tumor necrosis factor-α.

* Correspondence to: Department of Nursing, National Taichung University of Science and Technology, No. 193, Section 1, Sanmin Rd., Taichung 402 Taiwan.
** Correspondence to: Department of Veterinary Medicine, National Chung-Hsing University, No. 145, Xingda Rd., South Dist., Taichung 402, Taiwan.
E-mail addresses: wtj@nutc.edu.tw (T.-J. Wang), chenjr@email.nchu.edu.tw (J.-R. Chen).

https://doi.org/10.1016/j.brainresbull.2022.02.017
Received 8 December 2021; Received in revised form 11 February 2022; Accepted 22 February 2022
Available online 25 February 2022

different processes in different periods. Animal studies have indicated that if embryos are exposed to alcohol in the first trimester, their facial abnormalities and brain size would change significantly; if they are exposed to alcohol in the third trimester, behavioral deviations are more likely to be observed (Petrelli et al., 2018). Consequently, damage to the central nervous system (CNS) also leads to difficulties, with up to 90% of human children with FASD showing symptoms of hyperactivity and impulsivity (Wilhoit et al., 2017). Although there is no cure for FASD now, early intervention and lifelong support help children born with FASD cope with the difficulties that come with it (Zhang et al., 2018).

Recent studies have found that oxidative stress in fetal tissues is closely related to the development of FASD. Nicotinamide adenine dinucleotide (NADH) produced during the conversion of ethanol to acetate, which leads to a reduction in antioxidative capacity in prenatal/neonatal exposure of ethanol in animal or human (Brocardo et al., 2011). Besides, exposure to alcohol during the embryonic period of mice can also increase the level of malondialdehyde (MDA) and hydrogen peroxide (H_2O_2) in the brain (Zheng et al., 2014). It is important that the antioxidant defense system of the brain is somewhat limited. The activities of antioxidant enzymes, such as superoxide dismutase (SOD), catalase (CAT), and glutathione peroxidase (GPx), are lower in the brain of animals and humans with FASD than in other organs. (Brocardo et al., 2011; Zheng et al., 2014).

Ethanol can cross the blood-brain barrier (BBB) and directly affect the CNS, leading to neuroinflammation. Numerous other studies demonstrate that ethanol, as a pro-inflammatory trigger, would induce a neuroinflammatory response in the adult and developing CNS, such as the activation of microglia and astrocytes (Kane and Drew, 2021; Qin and Crews, 2012; Topper et al., 2015). Due to the activation of nuclear factor kappa-light chain enhancer of activated B cells (NF-κB) and the mitogen-activated protein kinase signaling pathway in microglia and astrocytes under exposure of ethanol, the expression of inducible nitric oxide synthase (iNOS) would increase (Blanco et al., 2004; Deng and Deitrich, 2007; Kane and Drew, 2021). Activated microglia or astrocytes also released pro-inflammatory cytokines, chemokines, and reactive oxygen species (ROS), which further lead to neuronal death, reduced neurogenesis, and altered synaptic plasticity (Kane and Drew, 2021; Qin and Crews, 2012; Topper et al., 2015; Wong et al., 2017). Furthermore, ethanol also disrupts the functions of the hippocampus by directly interacting with hippocampal neurons and its afferents (White et al., 2000). Besides, when the environment of the hippocampus deteriorates, such as inflammatory response and increased oxidative stress, hippocampal neurons will also be damaged. Presently, many studies all consider that the dendrites of pyramidal neurons changed their structure or lost function along with the environmental change in the hippocampus. And the change in the number of spines as excitatory synapses on the dendrites is the most obvious. This kind of change in the CA1 and CA3 region of the hippocampus would affect learning abilities and memory function (McDermott et al., 2006; Moser et al., 1994). For instance, some literature has shown that rats' pyramidal neurons in the hippocampus exposed to ethanol would change their morphologies and reduce the dendritic spine density, leading to cognitive impairment (Elibol-Can et al., 2014; Gil-Mohapel et al., 2010).

AST is a kind of carotenoid pigment found in the marine world of algae and aquatic animals. AST possesses potent antioxidant activity in the presence of hydroxyl and keto endings on each ionone ring. According to research, astaxanthin has powerful biological activities, like antioxidant, anti-inflammatory, and anti-apoptotic properties (Galasso et al., 2018). Because AST treatment has no apparent side effect and can act on the CNS by crossing the BBB (Guerin et al., 2003; Wang et al., 2015), research on the effects of AST in CNS diseases is extensive, recently. For instance, published reports have suggested that AST successfully reduced oxidative stress and inflammation, thus improving the symptoms of CNS diseases in diabetic rat model, subarachnoid hemorrhage-induced early traumatic brain injury rat model, D-galactose-induced brain aging rat model and FAB-induced Alzheimer's disease rat model. (Chen et al., 2021; Wang et al., 2019; Wu et al., 2014a, 2014b; Yeh et al., 2016). However, the efficacy of AST treatment on FASD is currently unclear. In light of the above, this study proposed to explore whether AST treatment can ameliorate morphological changes in hippocampal pyramidal neurons and cognitive impairment in FASD rats by reducing oxidative stress and neuroinflammatory response in the brain.

2. Materials and methods

2.1. Animals

Forty male rat pups, born to eight female Sprague-Dawley rats (BioLASCO, Taiwan), were used in this study. All the pups were assigned to four groups: 10 normal pups were control group (Con), 10 normal pups with the AST treatment group (Con+AST), 10 ethanol-inhaled pups were FASD group (FASD), and 10 ethanol-inhaled pups with the AST treatment group (FASD+AST). The day of birth was regarded as P1. The FASD induction was started on P2 and continued until P10. To investigate the effects of AST in a FASD rat model, AST treatment was administered on P53 and kept up until sacrifice (Fig. 1A). Subsequently, all the pups were sacrificed on P60. To determine the blood alcohol concentration (BAC) increased by alcohol vapor, 1.5 ml of whole blood from the tail vein of 12 female rats weighing 350–400 g would be taken 30 min after 1, 2 and 3 h of exposure to ethanol, respectively. Blood samples were sent to the Union Reference Laboratory (Taichung, Taiwan) to measure BAC (the maximum detection limit for BAC is 300 mg/dl. When the detection value is greater than the limit, it was recorded as 300 mg/dl). The animals were housed and cared for in a constant and comfortable environment (temperature: 24 ± 1 ℃; humidity: 60 ± 5%; light: 12/12 h light-dark cycle) according to the guidelines of the Animal Research Committee of the National Chung-Hsing University. Furthermore, all experiments adhered to the guidelines on ethical use of animals of the Taiwan National Science Council and all efforts were made to minimize the number of animals used and their suffering.

2.2. FASD rat model

An ultrasonic mist maker (JH-204-OT1-T, Zaihong technology Co, Taiwan) which was used to process liquid atomization (1.2 L/h), converted 65% ethanol (dilute with DDW) into ethanol mist. Mother rats and their pups were transferred to an alcohol exposure cage ($44 \times 42 \times 22\ cm^3$) at 9:00 a.m., starting at P2 and continuing until P10. To increase the survival rate, the time of ethanol exposure gradually rose: 0.5 h at P2, 1 h at P3 and P4, 1.5 h at P5, 2 h at P6 and P7, 2.5 h at P8, and 3 h at P9 and P10 (Fig. 1B). After the exposure was finished, the mother rats and pups were moved back into their original cages.

2.3. Astaxanthin (AST) treatment

10 mg AST (Sigma-Aldrich, St. Louis, MO, USA) was dissolved in 1 ml of normal saline with 0.5% DMSO and stored at 4 ℃ in the dark. The AST solution was mixed first before starting treatment. The pups were treated with AST (10 mg/ml/kg body weight/day) by intraperitoneal injection at 9:00, starting with P53 and continuing until P60. The behavioral test and sacrifice were performed 1 h after AST treatment.

2.4. Morris water maze (MWM) task

The methodology of the MWM task was used as described by Chen et al. (2021) and slightly adjusted to it. Rats would do this MWM task on P56 and run for 3 consecutive days (Fig. 1A). The water maze was a circular pool with a diameter of 145 cm and a depth of 52 cm. There were different visual makers (triangle, round, square, and star

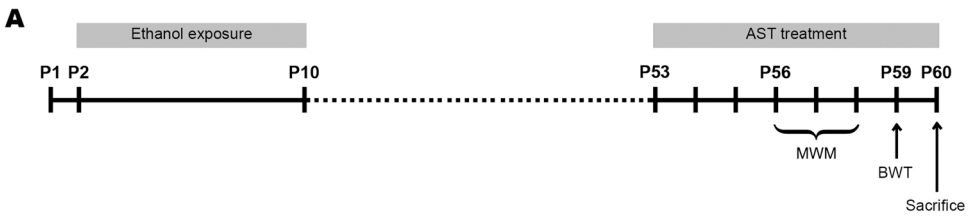

B

Postnatal days	1	2	3	4	5	6	7	8	9	10
Ethanol exposure time (h)	0	0.5	1	1	1.5	2	2	2.5	3	3

Fig. 1. Experiment design and ethanol exposure plan. Time schedule of experiments within postnatal 60 days was shown in A. Ethanol exposure plan (B) displayed the ethanol exposure time of postnatal 2–10 days. P, postnatal day; AST, astaxanthin; MWM, Morris water maze; BWT, beam walking test.

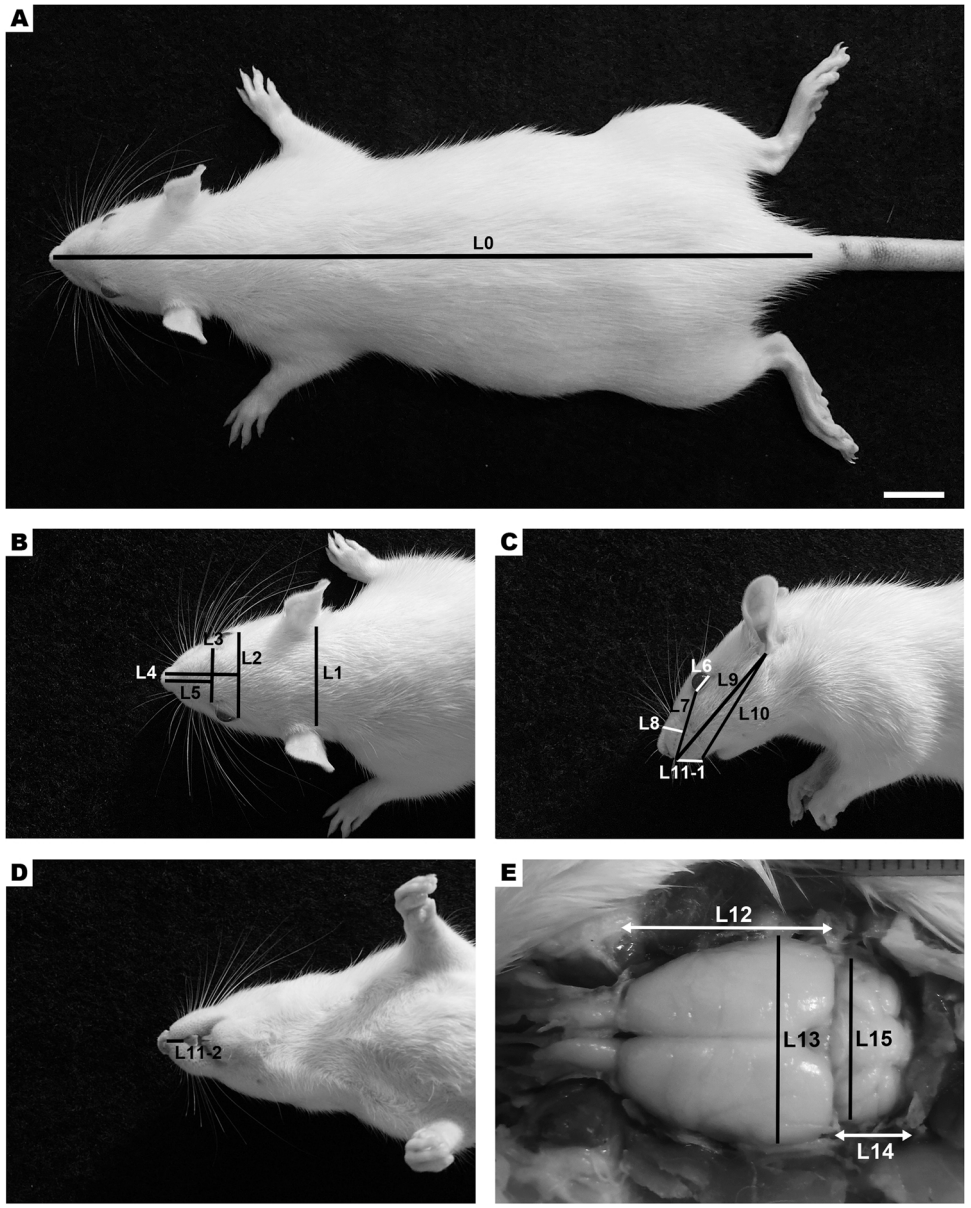

Fig. 2. Measurement parameters of rat's exterior, facial characteristics, and the cerebrum and the cerebellum. The exterior of the rat (A) and facial characteristics (B-D), and the cerebrum and the cerebellum (E) were shown. Parameters (L0-L15) indicated the location of measurement, respectively. Bar = 2 cm in A and 0.5 cm in B-D.

cardboards) on the edge of the pool. A circular transparent platform with a diameter of 24 cm and a height of 20 cm was placed 3 cm under water. This task was divided into two phases, acquisition test and probe test, respectively. The swimming paths of the animals were recorded with a digital camera and analyzed with the SMART video tracking system (SMART 3.0 V, Panlab, Harvard Apparatus, Cambridge, UK).

2.4.1. Acquisition test

In the acquisition test, rats would be allowed to swim and find the platform in the water maze for 3 consecutive days, and there were three trials per day. Each trial would have an interval of 10 min for the rats to rest. The rats were placed in a pool at random positions facing the edge of the pool. The trial was terminated immediately after the rat arrived on the platform and the rat was permitted to remain on the platform for 60 s and then return to their cage to wait for the next trial. If the rat did not find the platform in 180 s, the swimming time was recorded as 180 s and it was guided to stay on the platform for 60 s. Data from three trials of latency to the platform and swimming distance each day were averaged and analyzed.

2.4.2. Probe test

In the probe test, the transparent platform was removed from the pool and the pool divided into four equal quadrants. An hour after the acquisition test on the third day was completed, the rats would be allowed to swim again in 90 s. The swimming track, the swimming distance and time spent in the target quadrant were analyzed.

2.5. Beam walking test (BWT)

The protocol of BWT was referred to previously published report (Feng et al., 2014) and slightly adjusted to it. Animals were taking BWT on P59 (Fig. 1A). Rats were put on the platform, which was 10 × 10 cm^2 with a height of 52 cm. The wooden beams were 64 cm in length and had three widths of 3 cm, 2 cm, and 1 cm (Fig. 5A). During the test, rats needed to pass through the beam to the target platform on another side. To encourage the rats to pass the beam, a light was set at the start of the beam and a dark room was set at the end. In the training phase, animals passed through beams of different sizes in sequence (3 cm, 2 cm, and 1 cm in width), and once for each beam. After all rats were ensured that they could pass through the 1 cm width of beam, the formal phase began. In the formal phase, rats had three trials to pass through the 1 cm width of the beam within 60 s. To eliminate odor and residue, the beams were carefully cleaned with 75% alcohol each trial. During this process, the camera was set to record the number of foot faults in the right hindlimb and the spending time. If the animals fell from the beam during the crossing, the timing would be suspended immediately. After the animals were placed at the site where they fell, the timing would continue. In addition, if the rat did not arrive at the platform on another side within 60 s, the spending time was recorded as 60 s

2.6. Animal sacrifice and tissue preparation

On P60, rats were weighed and deeply anesthetized with 7% chloral hydrate mixed with 0.02% xylazine (0.5 ml/100 g body weight). After deep anesthesia, all rats were photographed with a camera to record their body length and facial characteristics, including dorsal view, lateral view, and ventral view (Fig. 2) (Anthony et al., 2010). The dorsal view of the cerebrum and cerebellum was also recorded after sacrifice and opening the cranium. Half of the animals would be used for intracellular dye injection, immunohistochemical and histochemical stainings, while the other half would be used for oxidative stress analysis. Tissue preparation for intracellular dye injection and immunohistochemical stainings referred to previously published protocols (Chen et al., 2021). Briefly, rats were transcardially perfused with 2% paraformaldehyde (PFA, Sigma-Aldrich) in 0.1 M phosphate buffer (PB), pH 7.3, about 500 ml for 30 mins. After perfusion, the cerebrums were removed and then sliced using vibratome (Technical Products International, St. Louis, MO, USA). A 1000 μm thick section was cut first in the 1.44 mm bregma of the cerebral cortex, containing the medial septal nucleus (MS), which was later used for immunohistochemistry. Furthermore, the cerebrum remains were divided into the right and left hemispheres. A 1000 μm thick section was cut on the − 2.7 mm bregma of the left hemispheres, including the dorsal hippocampal region, and then histochemistry was performed. Similarly, two 350 μm thick sections were sliced in the bregma − 2.7 mm of the right hemispheres, which were used for intracellular dye injection. The rest of the right hemisphere was then cut into a 1000-μm-thick section to proceed immunohistochemistry. The thick sections for histochemistry and immunohistochemistry were immediately post-fixed with 4% PFA in 0.1 M PB overnight at 4 ℃. The thick sections for intracellular dye injection were incubated with 10^{-7} M 4′,6-diamidino-2-phenylindole (DAPI) in 0.1 M PB for 30 mins at 4 ℃ to label cell nucleus. On the other hand, to preserve fresh hippocampus for the oxidative stress analysis, rat after deep anesthesia, they would be directly decapitated by a guillotine and immediately dissected. Using a hand-held homogenizer (Lab Gen 7, Cole Parmer) to homogenize and dilute hippocampus with the same weight of phosphate-buffer saline (PBS) solution and using a centrifuge (Pico 21, Thermo Fisher) to separate the supernatant at 9600 *g* for 20 mins at 4 ℃. Lastly, the supernatant was stored at − 80 ℃ for subsequent oxidative stress analysis.

2.7. Intracellular dye injection

The intracellular dye injection protocol was referred to previously published reports (Chen et al., 2017, 2014, 2021). After being stained with DAPI, the thick sections were placed on the stage of a fixed-stage

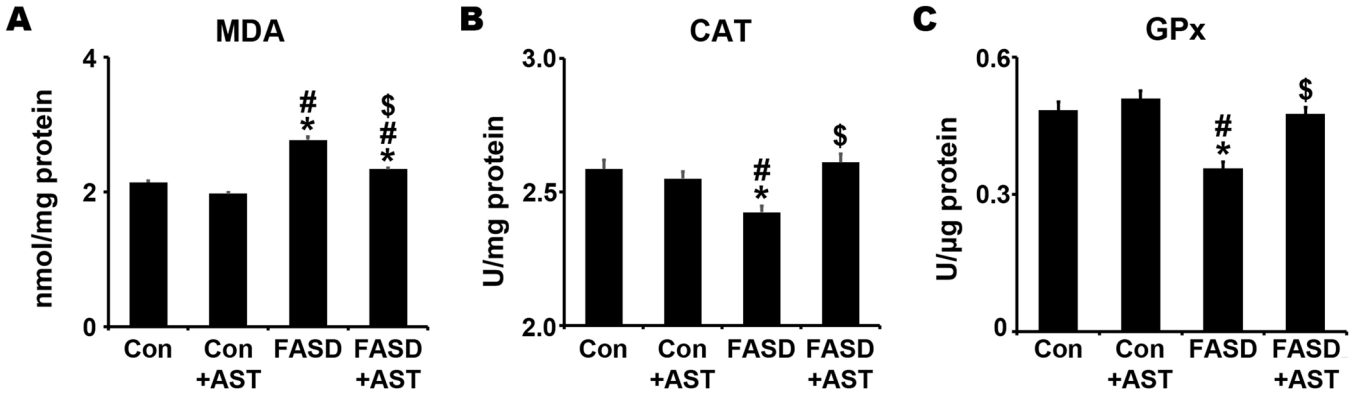

Fig. 3. Effects of AST treatment on MDA, CAT, and GPx activities of the hippocampus in the FASD rats. The levels of MDA (A), CAT (B), GPx (C) were analyzed and plotted. * , $p < 0.05$ between the marked and Con; #, $p < 0.05$ between the marked and Con+AST; $, $p < 0.05$ between the marked and FASD.

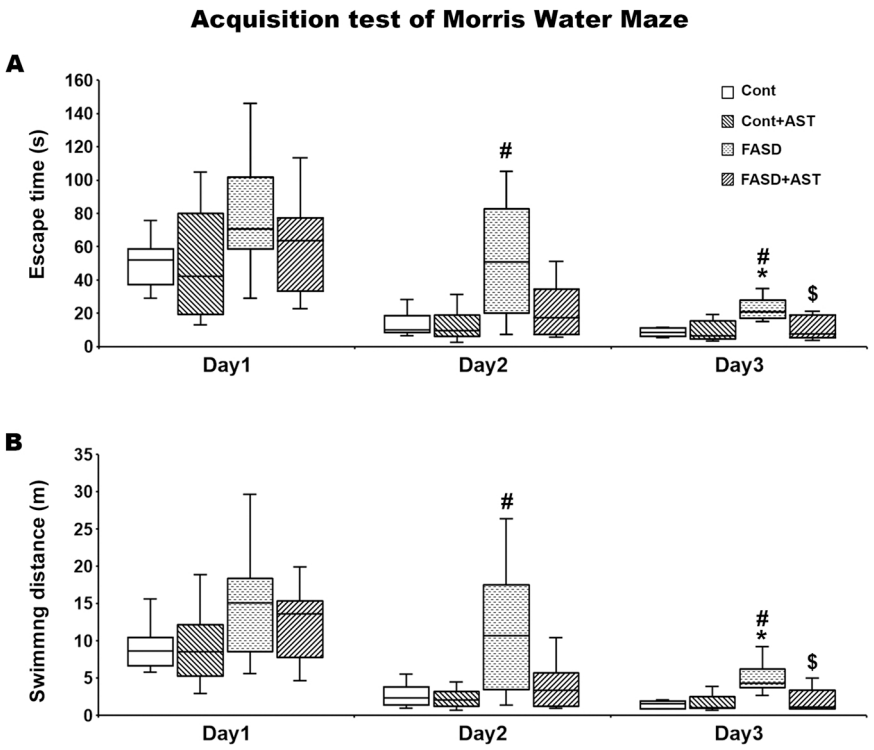

Fig. 4. Behavioral performances of the FASD rats in the acquisition test of MWM following the AST treatment. The escape time (A) and swimming distance (B) were analyzed and plotted. * , $p < 0.05$ between the marked and Con; #, $p < 0.05$ between the marked and Con+AST; $, $p < 0.05$ between the marked and FASD.

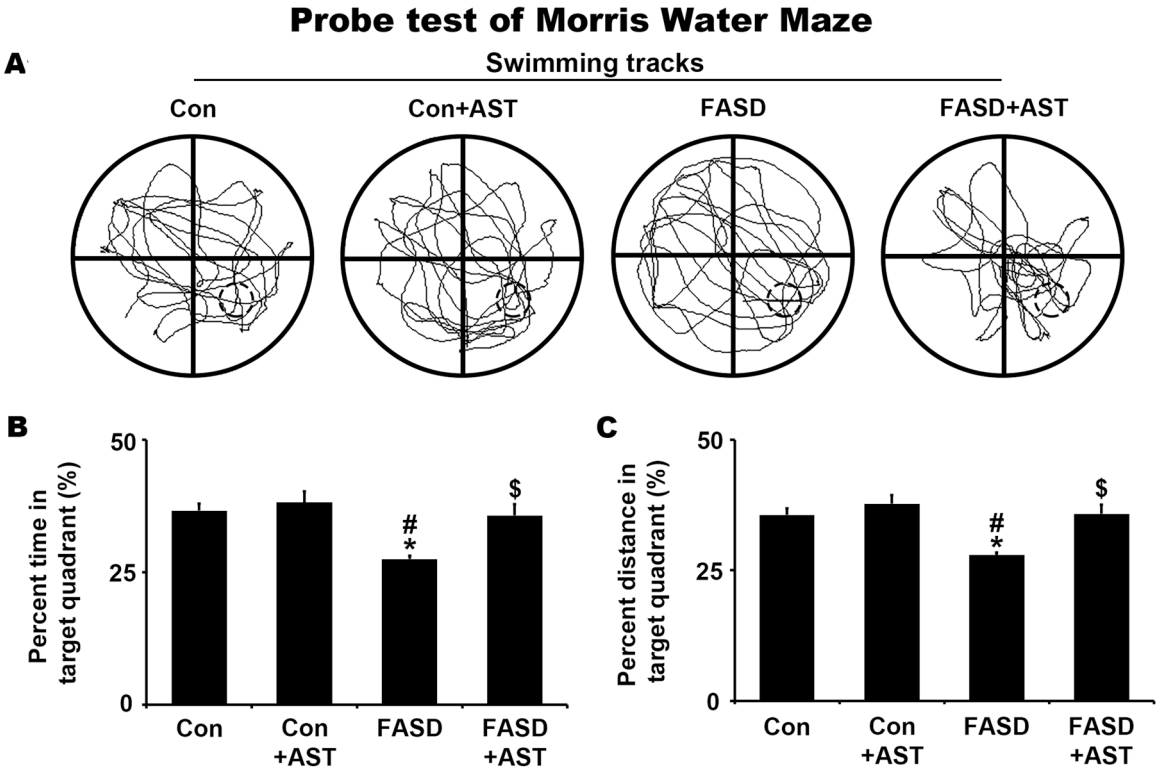

Fig. 5. Behavioral performances of the FASD rats in the probe test of MWM following the AST treatment. The swimming tracks of probe test (A), percentage of the swimming time in target quadrant (B), and percentage of the swimming distance in target quadrant (C) were analyzed and plotted. * , $p < 0.05$ between the marked and Con; #, $p < 0.05$ between the marked and Con+AST; $, $p < 0.05$ between the marked and FASD.

fluorescence microscope (BX51, Olympus, Japan). A three-axial hydraulic micromanipulator (Narishige, Japan) was used to control a glass micropipette filled with 4% Lucifer yellow (LY, Sigma-Aldrich) for intracellular injection. Five pyramidal neurons of the hippocampal CA1 region were randomly selected and injected LY for 3 min with an intracellular amplifier (Axoclamp–IIB, Axon, Foster City, CA, USA). Following the injection, the slice was postfixed with 4% PFA in 0.1 M PB overnight at 4 °C. 30% sucrose in 0.1 M PB solution was used to cryoprotect the thick sections for two days and the cryostat microtome was used to slice the tissue into 60-μm-thick serial sections and then collected individually orderly for subsequent immunoconversion of LY.

2.8. Tissue section

30% sucrose in 0.1 M PB solution was used to cryoprotect the thick sections for two days and the thick sections were sliced with a cryostat microtome (CM1850, Nussloch, Germany) into several 30-μm-thick sections. The cryosection of the hippocampus was sliced into 6 serial sections and collected for subsequent histochemical staining. The cryosection of MS nucleus was sliced in a set of 6 sections (one slice every three slices) and collected for subsequent immunohistochemical staining with ChAT to label ChAT+ neurons. Besides, the cryosection of right hippocampus was sliced in 15 serial sections, which were collected and divided into 5 sets orderly (one in every 5 sections of the series per set) for immunohistochemical staining with ionized calcium binding adaptor molecule 1 (Iba1), glial fibrillary acidic protein (GFAP), iNOS, neuronal nitric oxide synthase (nNOS) and ChAT to label microglia, astrocytes, iNOS+ neurons, nNOS+ neurons and ChAT+ fibers, respectively.

2.9. Histochemical staining

Senescence β-galactosidase staining kit (Cell Signaling Technology, USA) was used to distinguish senescent cells in the hippocampus and the protocol was in accordance with the instruction. Briefly, all sections of histochemical staining were washed with PBS, and they then were postfixed by fixative solution with 15 mins. After washing twice with PBS again, the sections were incubated with β-galactosidase staining solution at 37 °C overnight. Reacted sections were soaked in 70% glycerol one day and then were mounted on subbed slides, air-dried and coverslipped in Permount.

2.10. Immunohistochemistry and immunoconversion

All sections were immersed in 1% H_2O_2 (Kento chemical, Japan) and 0.2% Triton X-100 (Fisher scientific, USA) with 0.1 M PB for 1 h to offset endogenous peroxidase activity. Then, they was incubated with goat anti-Iba1 (1:1000, Abcam, Cambridge, UK), rabbit anti-GFAP (1:400, Abcam, Cambridge, UK), mouse anti-nNOS (1:1000, Santa Cruz Biotechnology, Santa Cruz, CA), mouse anti-iNOS (1:200, Santa Cruz Biotechnology, Santa Cruz, CA), goat anti-ChAT (1:500, EMD Millipore, USA), or biotinylated rabbit anti-LY (1:200, Thermo Fisher Scientific, USA), respectively, at 4 °C overnight. Thereafter, the sections were incubated with the secondary antibodies corresponding to the primary antibody, which were rabbit anti-goat (1:200, Vector Laboratories, USA), goat anti-rabbit (1:200, Vector Laboratories, USA) and horse anti-mouse (1:200, Vector Laboratories, USA) immunoglobulins, for 1 h at room temperature. Further, all sections were incubated with standard Elite ABC-HRP reagent (1:100, Vector Laboratories, USA) for 1 h at room temperature. 0.05% 3–3'-diaminobenzidine tetrahydrochloride (Sigma-Aldrich) and 0.01% H_2O_2 in 0.05 M Tris buffer allowed visualization of immunoreactivities. Afterwards, reacted sections were then mounted on subbed slides, air-dried and coverslipped in Permount.

2.11. Oxidative stress analysis

2.11.1. Thiobarbituric acid reactive substance (TBARS)

The method of TBARS was referred to previously published protocol (Ohkawa et al., 1979). An enzyme-linked immunosorbent assay (ELISA) reader (Asys UVM340, Biochrom, UK) was used to determine absorbance at 532 nm.

2.11.2. Catalase (CAT) and Glutathione peroxidase (GPx)

Using commercial Enzychrom™ Catalase Assay Kit (ECAT-100, BioAssay Systems, USA) and glutathione peroxidase (Ransel) assay (RS505, Randox Lab, UK) to detect CAT and GPx levels, respectively. Assays were performed according to the manufacturer's specifications using a microplate reader (Infinite F50, Tecan Co., Mannedorf, Switzerland).

2.12. Statistical analysis

Using Image-pro plus 6.0 (Media Cybernetics, USA) to measure the soma area and the relative IOD ration of cholinergic neurons in the MS nucleus and relative IOD ration of the cholinergic fibers in the hippocampus from 6 sections of the set in each rat. The relative IOD ration was normalized with data from the Con group. The densities of microglia, astrocytes, nNOS+ neurons were measured and iNOS+ neurons in a 10^5-μm^2 area of the dorsal hippocampus under primary motor cortex from 3 sections of the set and the densities of senescent cells in the same area as above from 6 sections of the set in each rat. To determine the density of dendritic spines on hippocampal CA1 pyramidal neurons, the dendrite of pyramidal neurons was divided into distal apical, proximal apical, and distal basal segments according to where the dendrites extend. 15 dendritic segments were randomly selected for each position of the dendrites of 5 randomly selected pyramidal neurons from each rat.

All data were checked for normality with observation of the data distribution and the Shapiro-Wilk normality test. The statistical significance of the MWM acquisition test was determined with Kruskal-Wallis one-way ANOVA of the nonparametric method followed by Dunn post hoc comparisons to find the differences between the groups, and the data were expressed as median (interquartile range, IQR = Q1 - Q3). The statistical significance of the MWM probe test, BWT, oxidative stress analysis, and morphological results were determined with one-way ANOVA of the parametric method followed by Tukey's post hoc comparisons to find the differences between groups and the data were expressed as mean ± SEM. $p < 0.05$ was considered significantly different.

3. Results

3.1. The effects of ethanol exposure and AST treatment on the BAC, weight, body length, facial characteristics, and characteristics of the cerebrum and the cerebellum of rats

3.1.1. BAC, Weight and body length

Alcohol vapor could successfully and stably introduce FASD in rats with minimal disturbance to mother and pups. BAC of adult female rats rose with increasing time of ethanol exposure (Table 1; $F = 49.32$, $p < 0.001$). Body weight ($F = 10.67$, $p < 0.001$) and length ($F = 9.73$,

Table 1
Blood alcohol concentration in different ethanol exposure time.

Ethanol exposure time	1 h	2 h	3 h
BAC (mg/dl)	152.3 ± 11.2	230.0 ± 10.7 *	290 ± 7.0 *#

One-way ANOVA followed by Tukey test:.
*, $p < 0.05$ between the marked and 1 h.
#, $p < 0.05$ between the marked and 2 h.

Table 2
Body weight & facial characteristics.

		Con	Con+AST	FASD	FASD+AST
Body weight (g)		340.2 ± 3.7	336.8 ± 2.7	311.7 ± 5.2 *#	331.5 ± 3.6$
L0	Body length (mm)	252.9 ± 2.8	251.4 ± 2.3	238.4 ± 1.3 *#	251.9 ± 2.0$
Facial morphometry (mm)					
L1	Binaural Distance	30.5 ± 0.8	29.6 ± 0.8	28.7 ± 0.5	29.5 ± 1.0
L2	Outercanthal Width	26.8 ± 0.4	26.8 ± 0.7	26.7 ± 0.6	25.6 ± 0.9
L3	Innercanthal Width	17.8 ± 0.5	17.1 ± 0.4	16.9 ± 0.3	16.6 ± 0.6
L4	Nasal Longer Length	30.3 ± 0.6	31.2 ± 0.9	28.8 ± 0.4	31.2 ± 1.3
L5	Nasal Bridge Length	21.9 ± 0.6	22.4 ± 0.8	19.9 ± 0.4	21.9 ± 1.3
L6	Palpebral Fissure	9.9 ± 0.5	9.7 ± 0.2	9.0 ± 0.3	9.6 ± 0.3
L7	Nasal Length	22.3 ± 0.4	23.3 ± 0.5	21.0 ± 0.4#	22.5 ± 0.3
L8	Nasal Depth	6.8 ± 0.2	7.1 ± 0.3	6.5 ± 0.2	6.8 ± 0.3
L9	Mid-facial Depth	48.4 ± 0.7	48.6 ± 0.8	45.1 ± 0.9 *#	48.3 ± 0.5$
L10	Lower-facial Depth	45.3 ± 0.7	45.2 ± 0.7	42.7 ± 1.0	45.5 ± 0.6
L11–1	Philtrum Length	6.0 ± 0.2	6.0 ± 0.3	4.6 ± 0.1 *#	5.5 ± 0.3
L11–2	Philtrum Length	5.8 ± 0.2	6.0 ± 0.3	4.6 ± 0.1 *#	5.4 ± 0.3
Brain morphometry (mm)					
L12	Cerebrum Length	16.4 ± 0.3	16.4 ± 0.4	14.7 ± 0.3 *#	14.9 ± 0.2 *#
L13	Cerebrum Width	15.3 ± 0.1	15.8 ± 0.3	14.0 ± 0.1 *#	14.3 ± 0.1 *#
L14	Cerebellum Length	5.6 ± 0.1	5.7 ± 0.1	4.9 ± 0.2 *#	4.9 ± 0.1 *#
L15	Cerebellum Width	12.3 ± 0.1	12.6 ± 0.4	10.8 ± 0.1 *#	11.1 ± 0.3 *#

One-way ANOVA followed by Tukey test:
*, $p < 0.05$ between the marked and Con
#, $p < 0.05$ between the marked and Con+AST
$, $p < 0.05$ between the marked and FASD

$p < 0.001$) in pups were measured before sacrifice (Table 2). The results showed that body weight ($p < 0.001$, FASD vs Con; $p < 0.001$, FASD vs Con+AST) and length ($p < 0.001$, FASD vs Con; $p = 0.001$, FASD vs Con+AST) in the FASD rat had been significantly reduced, but AST treatment could ease the reduction ($p = 0.006$ in body weight; $p < 0.001$ in body length, FASD+AST vs FASD). In addition, treating normal rats with AST would not affect their body weight and length ($p = 0.924$ in body weight; $p = 0.963$ in body length, Con+AST vs Con).

3.1.2. Facial characteristics

Facial characteristics were evaluated with 11 criterions by imaging from dorsal, lateral, and ventral of the rats (Fig. 2B-D). As shown in Table 2, the results of Con, Con+AST, FASD, and FASD+AST group were evaluated respectively. 3 criterions of facial characteristics had significant changes containing nasal length (Table 1 and Fig. 2C; L7, $F = 5.50$, $p = 0.004$), mid-facial depth (Table 2 and Fig. 2C; L9, $F = 5.62$, $p = 0.004$), and philtrum length (Table 2 and Fig. 2C and D; L11–1, $F = 6.62$, $p = 0.002$; L11–2, $F = 6.96$, $p = 0.001$). Mid-facial depth and philtrum length had significant differences between Con group and FASD group (Table 2; L9, L11–1 and L11–2, $p = 0.012$, $p = 0.004$ and $p = 0.005$, respectively, FASD vs Cont), showed that some facial characteristics could be influenced more easily by FASD. However, the recovery effect of AST treatment in FASD rats was limited, with only significant recovery in mid-face depth (Table 2; L9, L11–1 and L11–2, $p = 0.016$, $p = 0.120$ and $p = 0.097$, respectively, FASD+AST vs FASD).

3.1.3. Characteristics of the cerebrum and the cerebellum

The results of the measurements of the length and width of the cerebrums and the cerebellums after sacrifice were shown in Table 2 and Fig. 2E. The results of the Con, Con+AST, FASD, and FASD+AST group were evaluated respectively. All criterions of the cerebrum or the cerebellum were significantly changed including cerebrum length (Table 2; L12, $F = 10.59$, $p = 0.004$), cerebrum width (Table 2; L13, $F = 27.39$, $p < 0.001$), cerebellum length (Table 2; L14, $F = 8.25$, $p = 0.008$), and cerebellum width (Table 2; L15, $F = 13.03$, $p = 0.002$). All 4 criterions in FASD group were shorter than normal animals (Table 2; L12–15, $p = 0.012$, $p = 0.002$, $p = 0.037$ and $p = 0.011$ respectively, FASD vs Con), indicating severe growth retardation of both the cerebrum and the cerebellum. However, AST treatment in FASD could not recover the size of both the cerebrum and the cerebellum.

3.2. AST ameliorated the oxidative stress in FASD rats

The concentration of MDA, CAT, and GPx in the hippocampus was analyzed with ELISA. As shown in Fig. 3, the concentrations of MDA in Con, Con+AST, FASD, and FASD+AST group were 2.14 ± 0.04, 1.97 ± 0.02, 2.76 ± 0.06, and 2.34 ± 0.02 nmol/mg protein (Fig. 3A, $F = 77.50$, $p < 0.001$); the concentrations of CAT were 2.58 ± 0.03, 2.55 ± 0.03, 2.42 ± 0.02, and 2.61 ± 0.03 U/mg protein (Fig. 3B, $F = 8.52$, $p = 0.001$); the concentrations of GPx were 0.48 ± 0.02, 0.51 ± 0.02, 0.36 ± 0.01, and 0.48 ± 0.01 U/μg protein (Fig. 3C, $F = 17.28$, $p < 0.001$). In the hippocampus of FASD group, the concentration of MDA rose ($p < 0.001$, FASD vs Con; $p < 0.001$ FASD vs Con+AST), and the concentration of CAT and GPx decreased (CAT: $p = 0.005$, FASD vs Con; $p = 0.031$, FASD vs Con+AST; GPx: $p = 0.003$, FASD vs Con; $p < 0.001$, FASD vs Con+AST). However, after FASD rats were treated with AST, the concentration of MDA, CAT, and GPx restored ($p < 0.001$ in MDA, $p = 0.001$ in CAT and $p = 0.004$ in GPx, FASD+AST vs FASD). Therefore, AST treatment could ameliorate the oxidative stress caused by FASD.

3.3. AST ameliorated the spatial learning and memory defects in FASD rats

We appraised the spatial learning and memory of the animals with the MWM task for hippocampus-related functions (Figs. 4 and 5). And the acquisition test indicated that the escape latencies and the swimming distances of Con, Con+AST, FASD, and FASD+AST group progressively decreased in the 3 consecutive days (Fig. 4A and B). In the acquisition test, the escape latencies of normal rats were 51.9 (IQR= 37.1–58.4), 10.1 (IQR= 8.4–18.4) and 8.3 (IQR= 6.2–11.2) s for the 1st, 2nd, and 3rd day (Fig. 4A, Con); the escape latencies of normal rats with AST treatment were 42.3 (IQR= 19.3–80.0), 9.6 (IQR= 6.0–18.9) and 6.4 (IQR= 4.7–15.3) s (Fig. 4A, Con+AST). While those of FASD rats were individually 70.5 (IQR= 58.4–101.7), 50.7 (IQR= 20.1–82.5) and 20.7 (IQR= 17.0–27.8) s (Fig. 4A, FASD). It took FASD rats with AST treatment 63.5 (IQR= 33.4–77.4), 17.5 (IQR= 7.5–34.6) and 7.6 (IQR= 5.4–18.9) s to find the underwater platform (Fig. 4A, FASD+AST). In addition, the escape time on the 3rd day showed that FASD rats spent more time finding the underwater platform than normal rats ($p = 0.008$, FASD vs Con). And the escape time of FASD rats treated with AST on the 3rd day successfully reduced ($p = 0.018$, FASD+AST vs FASD).

Furthermore, the swimming distance in normal rats (Fig. 4B, Con) spent 8.6 (IQR= 6.6–10.5), 2.3 (IQR= 1.4–3.8) and 1.5 (IQR= 0.9–1.9) m separately finding the platform for the 1st, 2nd, and 3rd day of the 3 consecutive days of tests. The normal rats treated with AST were 8.5 (IQR= 5.3–12.2), 2.0 (IQR= 1.2–3.2) and 1.0 (IQR= 0.9–2.5) m respectively (Fig. 4B, Con+AST). While those of FASD rats were individually 15.1 (IQR= 8.5–18.4), 10.7 (IQR= 3.4–17.5) and 4.3 (IQR= 3.7–6.2) m (Fig. 4B, FASD). And it took FASD rats with AST treatment 13.7 (IQR= 7.7–15.4), 3.3 (IQR= 1.2–5.7) and 1.1 (IQR= 0.9–3.3) m to find the underwater platform (Fig. 4B, FASD+AST). Besides, the

swimming distance on the 3rd day showed that FASD rats took more swimming distance to find the platform than Con rats ($p = 0.003$, FASD vs Con). And the swimming distance of FASD rats treated with AST on the 3rd day successfully decreased ($p = 0.005$, FASD+AST vs FASD).

Finally, at the end of the MWM task, we utilized the spatial probe test to evaluate animals' performance in spatial memory (Fig. 5). During probe tests, when animals had a strong memory of the position of the underwater platform, they would leave more swimming tracks in the target quadrant, otherwise, they would explore around the edge of the pool (Fig. 5A). In the target quadrant, the ratio of swimming time (Fig. 5B) was 36.6 ± 1.4% in Con, 38.2 ± 2.1% in Con+AST, 27.5 ± 0.6% in FASD, and 35.8 ± 2.1% in FASD+AST, individually ($F = 6.16$, $p = 0.002$). While the ratio of swimming distance in target quadrant (Fig. 5C) was 35.6 ± 1.2 in Con, 37.7 ± 1.6 in Con+AST, 27.9 ± 0.4 in FASD, and 35.8 ± 1.7 in FASD+AST, separately ($F = 7.59$, $p < 0.001$). All of the above expounded that FASD rats performed poorer spatial memory ($p = 0.008$ in the ratio of swimming time and $p = 0.006$ in the ratio of swimming distance, FASD vs Con), while FASD+AST group performed better than FASD group and almost as well as Con group ($p = 0.040$ in the ratio of swimming time and $p = 0.012$ in the ratio of swimming distance, FASD+AST vs FASD; $p = 0.987$ in the ratio of swimming time and $p = 0.999$ in the ratio of swimming distance, FASD+AST vs Con).

3.4. AST treatment improved the sensorimotor integration in FASD rats

By analyzing the time required to reach the goal and the number of foot faults in Con, Con+AST, FASD, and FASD+AST group respectively with the BWT, the ability of sensory motor integration of different group of rats were evaluated (Fig. 6). The time different group of rats required to reach the goal (Fig. 6B) were 11.3 ± 0.7, 10.7 ± 1.7, 42.9 ± 7.2, and 21.5 ± 4.5 s ($F = 12.07$, $p < 0.001$); the number of foot faults (Fig. 6C) were 1.5 ± 0.3, 1.3 ± 0.6, 9.3 ± 1.6, and 4.2 ± 1.4 times ($F = 10.89$, $p < 0.001$). Both criterions showed that the rats in FASD group had poorer abilities of sensory motor integration ($p < 0.001$ in the time required to reach the goal and $p < 0.001$ in the number of foot faults, FASD vs Con). The performance of FASD rats after being treated with AST significant improved in both criterions ($p = 0.014$ in the time required to reach the goal, and $p = 0.026$ in the number of foot faults, FASD+AST vs FASD). Therefore, AST treatment could reduce the damage to the ability of sensory motor integration caused by FASD.

3.5. AST treatment improved the neuroinflammatory responses in FASD rats

To determine the extent of the neuro-inflammatory responses in the hippocampal CA1 region, antibodies of Iba1 and GFAP were used to label microglia (Fig. 7A-E, $F = 9.81$, $p < 0.001$) and astrocyte (Fig. 7F-J, $F = 22.12$, $p < 0.001$) in immunohistochemical staining. The density of microglia in the hippocampal CA1 region in the Con group was 13.5 ± 0.7 per 10^5 μm^2 (Fig. 7A). And the normal animals treated with AST had a density of microglia of 14.3 ± 0.9 per 10^5 μm^2 (Fig. 7B). While the density of microglia of the FASD rats significantly increased to 18.0 ± 0.5 per 10^5 μm^2 (Fig. 7A, C and E; $p < 0.001$, FASD vs Con). However, the FASD animals with the AST treatment successfully reduced it to 14.1 ± 0.4 per 10^5 μm^2 (Fig. 7C, D and E; $p = 0.004$, FASD+AST vs FASD) and close to Con level (Fig. 7A, D and E; $p = 0.895$, FASD+AST vs Con). Furthermore, the density of astrocytes in Con groups in the CA1 region of the hippocampus was 23.2 ± 0.4 per 10^5 μm^2 (Fig. 7F). And the normal animals treated with AST had an unchanged density of astrocytes of 23.1 ± 1.1 per 10^5 μm^2 (Fig. 7F, G and J; $p = 0.999$, Con+AST vs Con). While the density of astrocytes of the FASD rats significantly increased to 31.3 ± 0.8 per 10^5 μm^2 (Fig. 7F, H and J; $p < 0.001$, FASD vs Con). Otherwise, the FASD animals with the AST treatment successfully reduced it to 25.8 ± 0.9 per 10^5 μm^2 (Fig. 7H, I and J; $p = 0.001$, FASD+AST vs FASD).

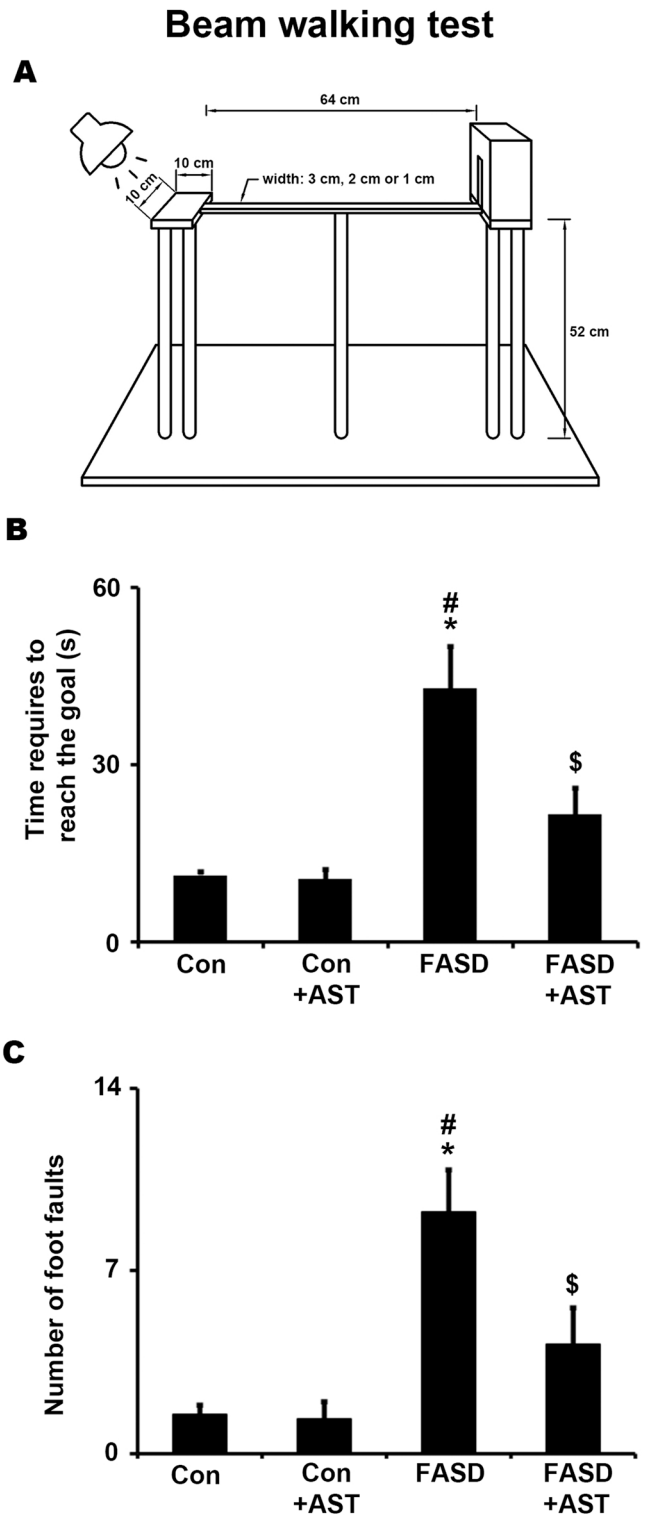

Fig. 6. Behavioral performances of the FASD rats in the beam walking test following the AST treatment. The equipment specification of the beam walk test was shown in A. Time required to reach the goal (B) and number of foot faults (C) were analyzed and schemed. * , $p < 0.05$ between the marked and Con; #, $p < 0.05$ between the marked and Con+AST; $, $p < 0.05$ between the marked and FASD.

The iNOS+ neurons (Fig. 8A-E, $F = 12.58$, $p < 0.001$) in the hippocampal CA1 region were observed. The density of iNOS+ neurons was 1.7 ± 0.2 per 10^5 μm^2 in the Con group (Fig. 8A), and it remained low density in the Con+AST group (Fig. 8B; 2.7 ± 0.2 per 10^5 μm^2). But it

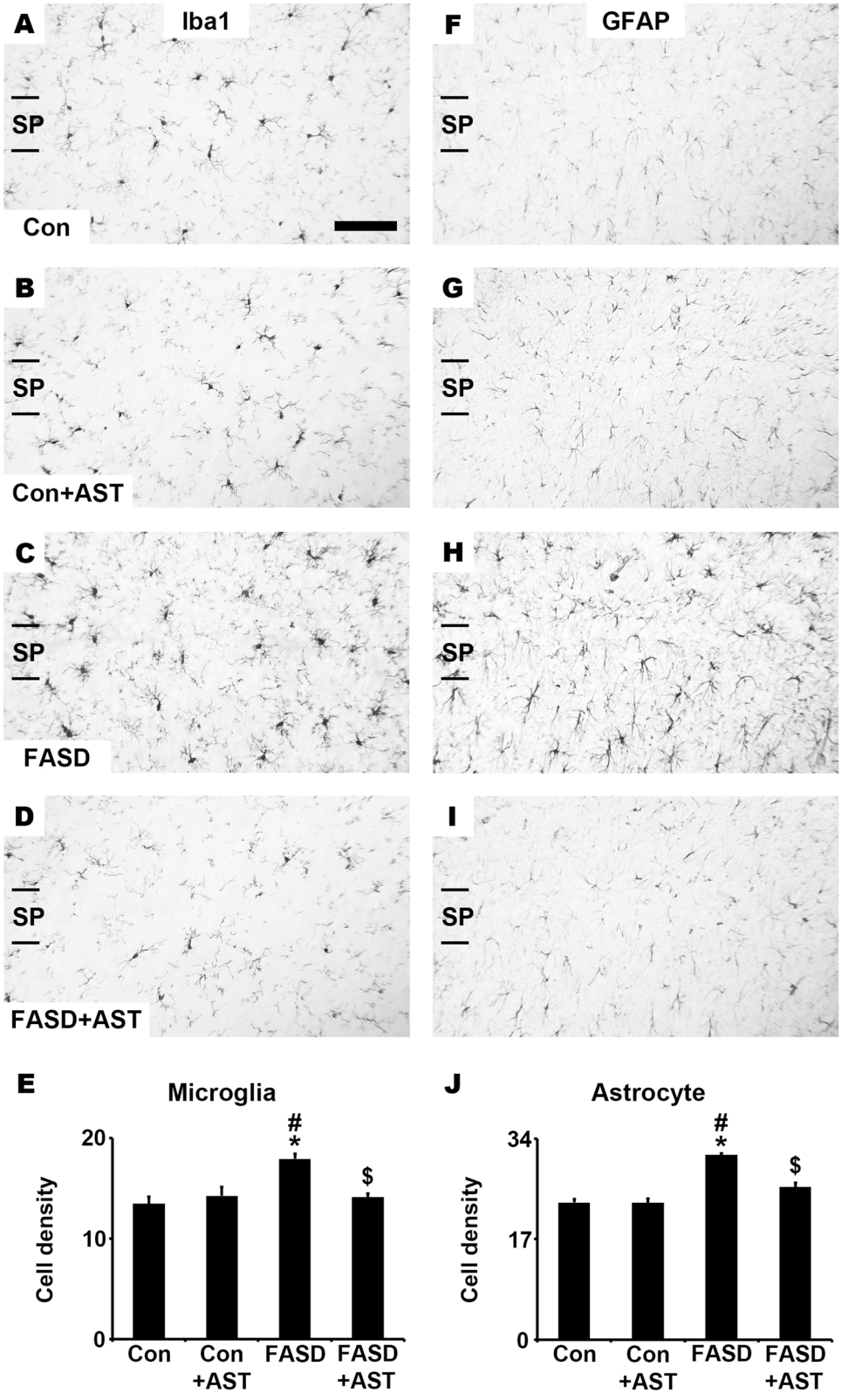

Fig. 7. Effects of AST treatment on the activation of microglia and astrocyte in hippocampal CA1 region of the FASD rats. Immunohistochemical stainings of the microglial marker Iba1 (A-D) and the astroglial marker GFAP (F-I) in the CA1 region of each group were illustrated. The densities of the labeled microglia (E) and astrocytes (J) in 10^5 μm^2 were counted and analyzed. * , $p < 0.05$ between marked and Con; #, $p < 0.05$ between marked and Con+AST; $, $p < 0.05$ between marked and FASD. SP, stratum pyramidale. Bar = 100 μm for all micrographs.

increased significantly to 4.0 ± 0.4 per 10^5 μm^2 in the FASD group (Fig. 8A, C and E; $p < 0.001$, FASD vs Con). With the treatment of AST, the FASD rats had the density of iNOS+ neurons reduced (Fig. 8C, D and E; 2.0 ± 0.3 per 10^5 μm^2 in FASD+AST; $p = 0.001$, FASD+AST vs FASD) and close to Con level (Fig. 8A, D and E; $p = 0.934$, FASD+AST vs Con). SA-β-galactosidase staining was used to label senescent cells in the hippocampal CA1 region (Fig. 8F-J, $F = 31.51$, $p < 0.001$), which indicated that these cells might temporarily stop their functions and release inflammatory factors. In normal rats, only a few SA-β-gal+ cells were present in the hippocampal CA1 region whether AST treatment or not (Fig. 8F and G; 0.6 ± 0.2 per 10^5 μm^2 in Con and 0.6 ± 0.1 per 10^5 μm^2 in Con+AST, respectively). While, the density of SA-β-gal+ cells of

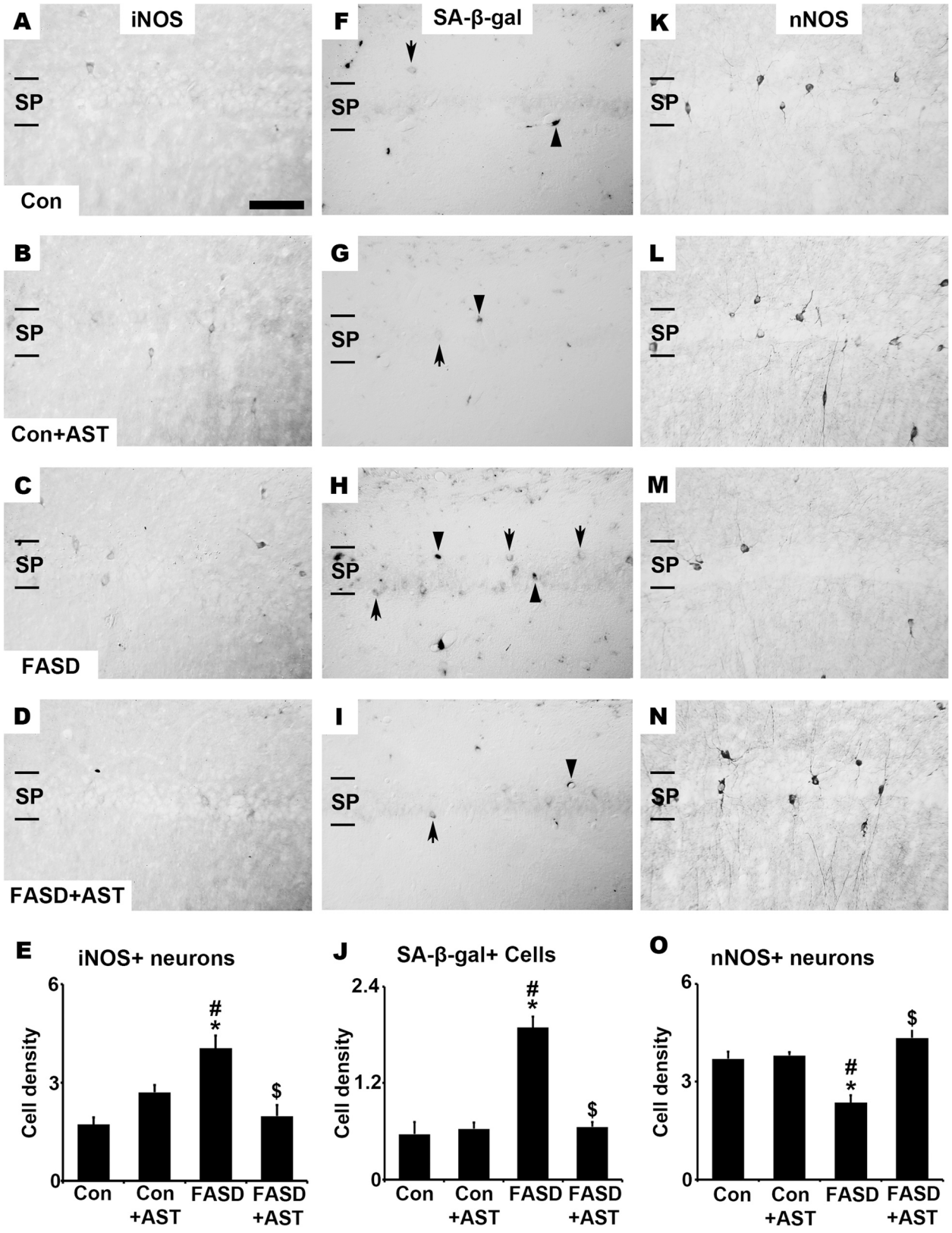

Fig. 8. Effects of AST treatment on the expression of iNOS, SA-β-gal and nNOS in hippocampal CA1 region of the FASD rats. Representative micrographs of the iNOS+ neurons (A-D), SA-β-gal+ cells (F-I) and nNOS+ neurons (K-N) in the CA1 region of each group were illustrated. The densities of the labeled iNOS+ neurons (E), SA-β-gal+ cells (J) and nNOS+ neurons (O) in 10^5 μm^2 were counted and analyzed. SA-β-gal+ cells were distributed in the capillary endothelial cell (arrowhead) and the neuron or neuroglia (arrow), and we only counted those in the stratum pyramidale. * , $p < 0.05$ between marked and Con; #, $p < 0.05$ between marked and Con+AST; $, $p < 0.05$ between marked and FASD. SP, stratum pyramidale. Bar = 100 μm for all micrographs.

the FASD rats significantly increased to 1.9 ± 0.1 per 10^5 μm^2 (Fig. 8F, H and J; $p < 0.001$, FASD vs Con). As speculated, the FASD animals with the AST treatment successfully reduced it to 0.7 ± 0.1 per 10^5 μm^2 (Fig. 8H, I and J; $p < 0.001$, FASD+AST vs FASD) and close to Con level (Fig. 8F, I and J; $p = 0.942$, FASD+AST vs Con). It indicated that SA-β-gal+ cells in FASD would become inactive through the AST treatment.

3.6. AST treatment restored the expression of nNOS in FASD rats

nNOS+ neurons (Fig. 8K-O, $F = 12.41$, $p < 0.001$) in the hippocampal CA1 region were observed. The density of nNOS+ neurons was 3.7 ± 0.2 per 10^5 μm^2 in the Con group (Fig. 8K), and it remained high density in the Con+AST group (Fig. 8L; 3.8 ± 0.1 per 10^5 μm^2). However, it dropped significantly to 2.35 ± 0.23 per 10^5 μm^2 in the FASD group (Fig. 8K, M and O; $p = 0.005$, FASD vs Con). With the treatment of AST, the FASD rat had the density of nNOS+ neurons increased (Fig. 8M, N and O; 4.34 ± 0.34 per 10^5 μm^2 in FASD+AST; $p < 0.001$, FASD+AST vs FASD).

3.7. Changes in cholinergic septo-hippocampal innervation in FASD rats and AST treatment

The cholinergic neurons in MS nucleus regulated the activity of neurons in the hippocampal CA1 region by their axon extending to the hippocampal CA1 region. Thus, the ChAT antibody in immunohistochemical staining was used to assay the immunoreactivity of cholinergic neurons in MS nucleus (Fig. 9 A-E and J). The soma area of cholinergic neurons in MS nucleus in Con, Con+AST, FASD and FASD+AST were 116.8 ± 3.1, 117.5 ± 1.5, 102.1 ± 0.8, and 111.7 ± 2.2 μm^2/cell (Fig. 9E, $F = 11.56$, $p < 0.001$). There was smaller soma area of cholinergic neurons in MS nucleus in FASD rat than normal rat (Fig. 9A, C and E; $p < 0.001$, FASD vs Con). Otherwise, FASD rats treated with AST would recover the soma area of cholinergic neurons in MS nucleus (Fig. 9 C, D and E; $p = 0.024$, FASD+AST vs FASD). The relative IOD ratio was also analyzed to indicate the total level of ChAT in cholinergic neurons of MS nucleus (Fig. 9J, $F = 15.60$, $p < 0.001$). The Con+AST group didn't alter the total level of ChAT in cholinergic neurons of MS nucleus (Fig. 9A, B and J; 99.3 ± 1.6% in Con+AST). However, FASD rats were exposed to ethanol after birth, resulting in a decrease in the total level of ChAT produced by the cholinergic neurons of MS nucleus (Fig. 9A, B, C and J; 86.8 ± 2.2% in FASD; $p = 0.001$, FASD vs Con+AST). After FASD rats were treated with AST, cholinergic neurons of MS nucleus would restore the expression of ChAT (Fig. 9C, D and J; 99.2 ± 1.6% in FASD+AST; $p = 0.001$, FASD+AST vs FASD). Furthermore, the distribution pattern of cholinergic fibers of cholinergic neurons (Fig. 9F-J; $F = 17.22$, $p < 0.001$), which were projected from the MS nucleus into the hippocampal CA1 region. The Con+AST group didn't alter the distribution pattern of cholinergic fibers in the hippocampal CA1 region (Fig. 9F, G and J; 100.3 ± 1.5% in Con+AST). The ethanol exposure after birth reduced the distribution pattern of cholinergic fibers in the hippocampal CA1 region (Fig. 9F, G, H and J; 60.5 ± 7.6% in FASD; $p < 0.001$, FASD vs Con+AST). With the treatment of AST, the FASD rats increased the cholinergic fibers in the hippocampal CA1 region (Fig. 9H, I and J; 82.4 ± 3.1% in FASD+AST; $p = 0.018$, FASD+AST vs FASD).

3.8. AST treatment restored the densities of dendritic spines on the hippocampal CA1 pyramidal neurons of FASD rats

We examined the densities of dendritic spines on hippocampal CA1 pyramidal neurons revealed with intracellular dye injection to investigate the morphological differences related to spatial learning and memory changes. The dendritic spine on pyramidal neurons, which was a dynamic structure, was the main site connected with afferent neurons and forming excitatory synapses. Spine density on distal apical dendrites (Fig. 10A and B) was 16.2 ± 0.7 spines/10 μm in Con group, 16.3 ± 0.1 spines/10 μm in Con+AST group, 11.8 ± 0.5 spines/10 μm in FASD group, and 15.1 ± 0.2 spines/10 μm in FASD+AST group, individually ($F = 24.67$, $p < 0.001$). In addition, spine density on proximal apical dendrites (Fig. 10C and D) was 17.6 ± 0.4 spines/10 μm in Con group, 17.5 ± 0.3 spines/10 μm in Con+AST group, 13.7 ± 0.3 spines/10 μm in FASD group, and 16.9 ± 1.1 spines/10 μm in FASD+AST group, individually ($F = 9.00$, $p = 0.006$). Whereas spine density on distal basal dendrites (Fig. 10E and F) was 15.8 ± 0.4 spines/10 μm in Con group, 15.3 ± 0.3 spines/10 μm in Con+AST group, 13.2 ± 0.2 spines/10 μm in FASD group, and 15.6 ± 0.4 spines/10 μm in FASD+AST group, individually ($F = 14.36$, $p = 0.001$). Spine densities of CA1 pyramidal neurons on the distal and proximal segments of the apical dendrites and distal basal dendrites were significantly decreased 27.4%, 22.1%, and 17.0% individually after the postnatal ethanol exposure, compared to Con group ($p < 0.001$ in apical distal dendrites, $p = 0.009$ in apical proximal dendrites, and $p = 0.002$ in basal distal dendrites, FASD vs Con). Otherwise, the AST treatment could significantly restore the spine densities on CA1 pyramidal neurons by 28.2%, 23.5% and 18.3%, respectively ($p = 0.003$ in apical distal dendrites, $p = 0.024$ in apical proximal dendrites, and $p = 0.003$ in basal distal dendrites, FASD+AST vs FASD).

4. Discussion

4.1. The effects of ethanol exposure in neurodevelopmental period

BAC in human mothers greater than 200 mg/dl could be the cause of severe FAS in the fetus, and even lower BACs can also lead to milder FASD (Patten et al., 2014). Human BAC of more than 200 mg/dl would cause impaired reflexes, reaction time, and syncope, and BAC of more than 400 mg/dl would even cause death (Petrelli et al., 2018). In this study, mother rats and pups were exposed to inhaled gaseous ethanol for progressive postnatal ethanol exposure for 9 days. BACs in adult female rats were checked for 1-, 2-, and 3-hour exposure to ethanol and were achieved in the range between 150 and 290 mg/dl. This progressive increase in ethanol exposure could increase the survival rate of the pups. During our experiments, we only observed poorer activity, reaction time, and reflex in mother rats and pups, but no immediate coma or death. However, after a few hours, these phenomena could be observed with a significant recovery. Many appearance characteristics of prenatal/postnatal alcohol exposure mice or rat models were consistent with the characteristics of human patients, such as craniofacial abnormalities, eye malformation, and growth retardation. These characteristics had been observed within the life cycle (Patten et al., 2014; Petrelli et al., 2018). In our FASD rat model, growth retardation and some changes in facial characteristics, such as nasal length, mid-facial depth, and philtrum length were observed.

The brain development which is characterized by large amounts of growth and differentiation occurs in the third trimester whether in human, mice, or rat (Dobbing and Sands, 1979; Mooney et al., 1996). Previous research used magnetic resonance imaging to examine the brain of the FASD human patient, and the results showed differences in the volume and thickness of the cerebral cortex, abnormal subcortical structures, including caudate nucleus, diencephalon, hippocampus, and structural abnormalities of cerebellum (Nunez et al., 2011). There were several different timings in the third trimester neurodevelopmental process between rats and humans (Watson et al., 2006): (1) Rat's peak brain growth as a percentage of adult body weight of rat occurred around P7–8 and brain growth spurt occurred from birth to 2 weeks after birth, while human's peak brain growth occurred at birth and brain growth spurt lasted 2–3 years; (2) Unlike human, rat acquired little prenatal myelination, and postnatal myelination in different brain regions ranged from P7–17; (3) Speculating with four parameters of brain development (63.2% adult synapses, glutamate decarboxylase activity, ChAT activity, and electrical activity), rat pups with P12–13 were equivalent to human neonates in aggregate. It was generally considered

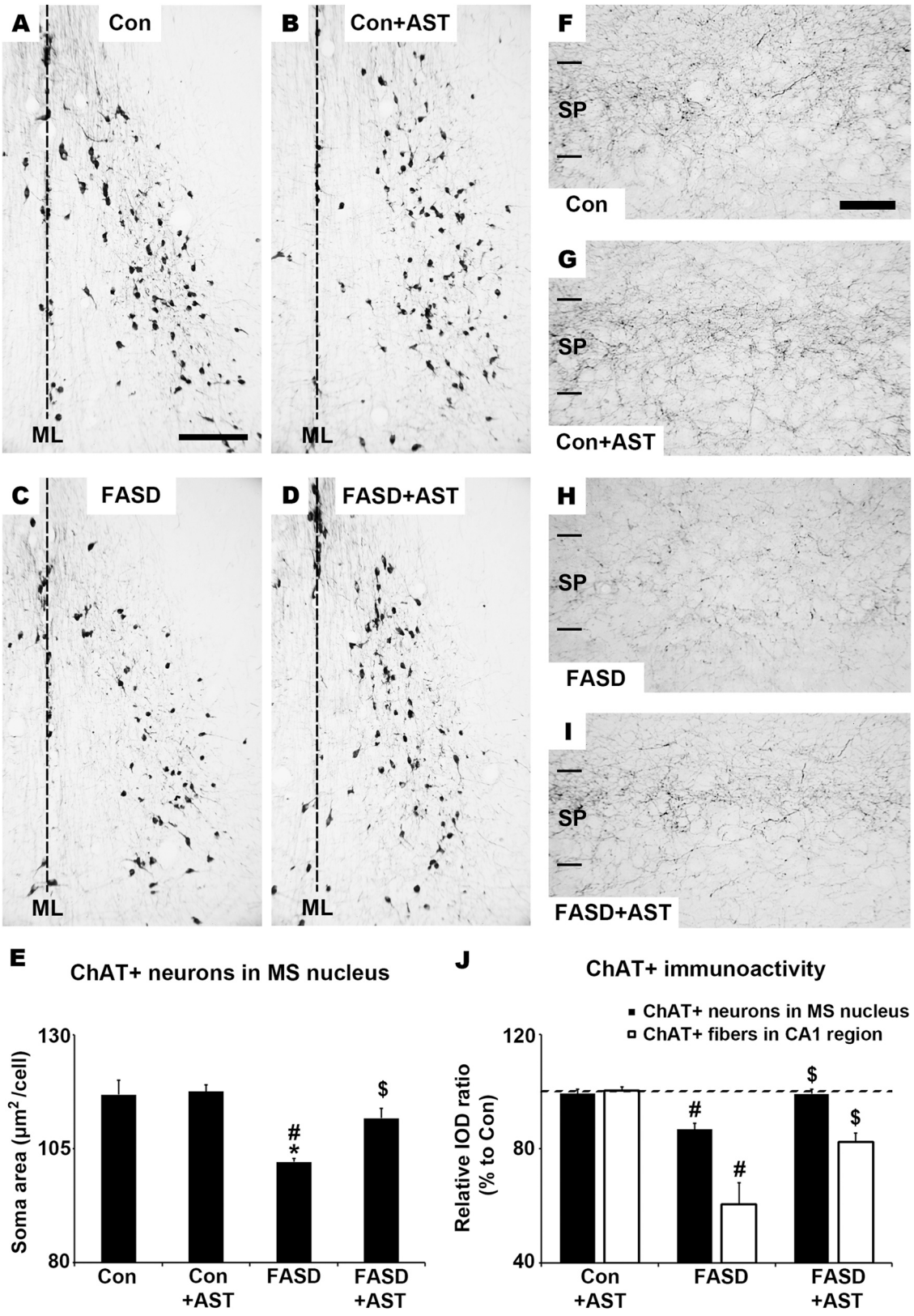

Fig. 9. Effects of AST treatment on cholinergic septo-hippocampal innervation of the FASD rats. Micrographs of the ChAT+ neurons in MS nucleus (A-D) and ChAT+ fibers in hippocampal CA1 region (F-I) of the four groups were illustrated. In the MS nucleus, the soma area was analyzed in E. The relative IOD ratio of ChAT+ neurons in the MS nucleus and ChAT+ fibers in the hippocampal CA1 region were respectively analyzed in J. * , $p < 0.05$ between marked and Con; #, $p < 0.05$ between marked and Con+AST; $, $p < 0.05$ between marked and FASD. ml, midline. Bar = 200 μm for all micrographs. Dotted lines in F and J indicated 100%.

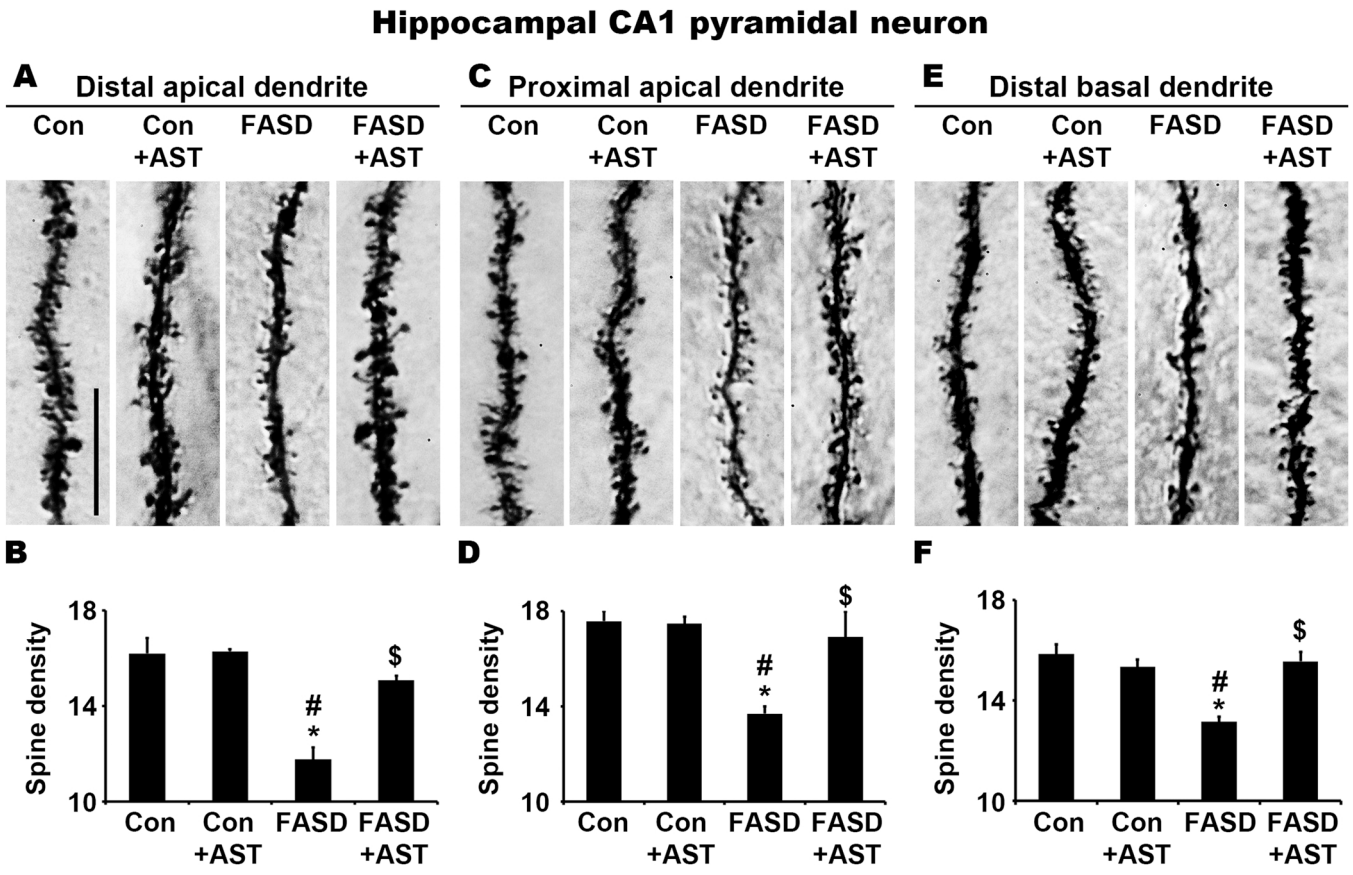

Fig. 10. Effects of AST treatment on the dendritic spine on the hippocampal CA1 pyramidal neurons of the FASD rats. Representative micrographs of the distal (A) and proximal (B) apical dendrites and distal basal dendrites (C) of the pyramidal neurons in hippocampal CA1 region from each group were illustrated. Spine densities per 10 μm of distal apical, proximal apical, and distal basal dendrites were analyzed and plotted in B, D and F, individually. * , $p < 0.05$ between marked and Con; #, $p < 0.05$ between marked and Con+AST; $, $p < 0.05$ between marked and FASD. Bar = 10 μm for all micrographs.

that P1–10 in rats or mice was comparable to the third trimester in human (Mooney et al., 1996); therefore, exposure to alcohol during this period could affect the development of the CNS. The published study had confirmed that exposure to alcohol in rats during the third trimester period could lead to hypoplasia of the CNS (Shabab et al., 2017). This study also observed a typical feature of microcephaly in FASD rats, with less length and width of cerebrum and cerebellum.

Besides, our detection in behavioral tests (MWM and BWT) also proved that the rat model could correctly simulate FASD. A study published in 2021 showed that the latency prenatal ethanol exposure rats required to reach the platform location increased; the number of entries into the platform location, the time in the platform quadrant, and the number of crossings in the platform quadrant decreased, which meant that the rats with FASD would show intelligence and cognitive impairment (Aglawe et al., 2021). Because alcohol exposure during development would impact the cerebellum, human children with FASD thus appeared to have many symptoms associated specifically with cerebellar deficits (Luo, 2015), such as sensory-motor functions (Hen-Herbst et al., 2020).

During ethanol metabolism, NADH would be generated and re-oxidized to NAD^+ in the mitochondria, which increased the generation of ROS. Furthermore, ethanol exposure might also reduce endogenous antioxidant activities, such as SOD, CAT, GPx, glutathione, and glutathione reductase. Unbalanced redox led to protein oxidation, lipid peroxidation, and DNA damage (Brocardo et al., 2011; Zheng et al., 2014). In our study, when rats are exposed to ethanol in their infancy, unbalanced redox in the hippocampus containing an increase in the level of lipid peroxidation level and decreased levels of SOD and GPx, could still be observed at 60 days of age. Therefore, it is inferred that exposure to ethanol during embryonic development or infancy may cause chronic oxidative stress in the CNS.

High oxidative stress in the CNS was often accompanied by a neuroinflammatory response, such as the activation or proliferation of microglia and astrocytes. Activated microglia and astrocytes triggered the PI3K/Akt/mammalian target of rapamycin (mTOR) or p38 mitogen-activated protein kinases (p38 MAPK) signaling pathway, which resulted in phosphorylation and ubiquitination of NF-κB, to transcript and translate the inflammatory cytokines, such as interferon-γ, tumor necrosis factor-α (TNF-α), interleukin (IL)− 1β, and IL-6, and chemokines, such as cyclooxygenase (COX)− 1, COX-2 and iNOS, and release them into intercellular substance, leading to neuronal loss or dysfunction (Blanco et al., 2004; Bogdan, 2001; Hatano et al., 2001; Kane and Drew, 2021; Shabab et al., 2017; Topper et al., 2015; Wong et al., 2017). Furthermore, mitochondrial dysfunction mediated by oxidative stress of microglia and astrocytes would generate more ROS ending in the vicious circle of chronic neuroinflammation (Brocardo et al., 2011; Kane and Drew, 2021). It should be noted that our result revealed that ethanol exposure during the developmental period would cause normal cells to express SA-β-galactosidase in the hippocampal CA1 region. Although there are still many controversies about SA-β-gal+ cells being senescent cells (Piechota et al., 2016). Many scholars believe that there are multiple factors that induce senescent cells, one of them was oxidative stress (Van Deursen, 2014). In addition to stopping the cell cycle, senescent cells have a typical feature of inducing the inflammatory transcriptome and secreted various senescence-associated secretory phenotype factors, including the pro-inflammatory factor IL-1β, IL-6 and IL-8 (Ito et al., 2017; Nacarelli et al., 2019; Sikora et al., 2021; Van Deursen, 2014). It might be one of the causes of chronic neuroinflammation in our FASD rat

model. Previous studies of FASD animal model, which indicated that the chronic neuroinflammatory response might contribute to the pathology related to FASD, corresponded to our study (Kane and Drew, 2021; Qin and Crews, 2012; Topper et al., 2015). Although rats were only exposed to ethanol for 9 days after birth, increased cell density of microglia, astrocytes, and iNOS+ neurons in hippocampal CA1 region were observed at P60, which revealed that there was a chronic inflammatory response, while the expression of inflammatory cytokines could lead to alteration of synaptic plasticity (Combs et al., 2001).

nNOS played an important role within neurons, including providing neuroprotection, catalyzing nitric oxide (NO) production, and participating in cellular signaling pathways (Han et al., 2010; Joca et al., 2019; Karacay et al., 2015; Picon-Pages et al., 2019). It is currently known that the expression of nNOS could provide neuroprotection against alcohol toxicity during neurodevelopment. The published research, which used $nNOS^{-/-}$ mice and performed postnatal alcohol induction, indicated that the lack of nNOS expression would lead to worsening of behavioral deficits, microcephaly, and neuronal losses after alcohol exposure (Karacay et al., 2015). Similar results have been observed in our study. Significant reduction of nNOS+ neurons in the hippocampal CA1 region could be observed in FASD-induced rats. It could be speculated that the neuroprotection provided by nNOS reduced in FASD rats, which made neurons more susceptible to neuroinflammation or oxidative stress. Additionally, NO catalyzed by nNOS also had many functions, including acting as a neurotransmitter, regulating blood vessel tension, participating intracellular signaling pathways, stabilizing synaptic connections, and forming dendritic spines (Charriaut-Marlangue et al., 2013; Joca et al., 2019; Picon-Pages et al., 2019).

Cholinergic neurons of MS projected their axons to the hippocampal CA1 region to modulate the hippocampal CA1 pyramidal neurons in synaptic connection and regulate their activity. Research previously discovered that cholinergic depletion in the MS was associated with impaired hippocampal-dependent learning and memory and reduced the number of branches of apical dendrites and spine densities on apical dendrites (Kanju et al., 2012; Robertson et al., 1998). The cholinergic lesion of forebrain reduced the complexity and spine density of CA1 pyramidal neurons and changed the glutamatergic synaptic transmission of the hippocampus related to the establishment of learning and memory (Frechette et al., 2009). Furthermore, studies investigated the influence of ethanol exposure on septohippocampal cholinergic projection neurons in MS and reported the loss of ChAT+ neurons in the septal area of fetal mice exposed to high doses of ethanol during early gestation (Swanson et al., 1996). In the present study, we found that the reduction in the expression of the cholinergic neuron in MS and the cholinergic terminals in the CA1 field of the hippocampus in the rat model of FASD, which represented that the function of the neurons in the MS nucleus that projected to the hippocampus decreased. Whether loss of cholinergic innervation is related to a decrease in synaptic homeostasis provided by nNOS remains to be proved by further experiments, but loss of cholinergic innervation can cause spine loss in cortical pyramidal neurons has been confirmed in many studies (Frechette et al., 2009; Garrett et al., 2006; Mandolesi et al., 2008).

4.2. The effects of AST treatment in FASD rats

Current research indicated that, after AST treatment, facial deformities and microcephaly would not improve in FASD rats. However, it was worth noting that the behavioral performance, oxidative stress, neuroinflammatory response and spine loss of CA1 pyramidal neurons in FASD rats improved significantly after AST treatment. AST was best known for its anti-oxidative and anti-inflammatory properties. Our results were in line with previous reports in which AST effectively improved the brain environment of the FASD rat through reduced oxidative stress (Zheng et al., 2014). Currently, there are many animal models of diseases in the CNS, such as stroke, subarachnoid hemorrhage, and AD, that have been shown to be able to take AST to reduce the oxidative stress in the brain (Chen et al., 2021; Shen et al., 2009; Wu et al., 2014a). AST utilized scavenging free radicals, reducing MDA in the body, increasing the activity of antioxidant enzymes, and regulating the expression of genes related to oxidative stress to prevent oxidative damage (Wu et al., 2015). For instance, AST supplementation could stimulate the performance of thioredoxin reductase, heme oxygenase-1 and nuclear factor erythroid-related factor 2 (Nrf2), and these factors had been shown to protect neurons from oxidative damage. They could activate the phosphoinositide 3-kinase (PI3K)/Akt pathway to increase the performance of phase II antioxidant enzymes and make Nrf2 nuclear translocation to protect specific neurons from oxidative damage induced by H_2O_2 (Li et al., 2013).

Meanwhile, AST reduced the density of activated microglia and astrocytes and the expression of iNOS in the hippocampus. This means successfully controlling the neuroinflammatory response in FASD rats after AST treatment. Because AST inhibited the gene expression of NF-κB signaling pathway, the activation of glial cells would be prevented (Lee et al., 2003). Furthermore, NF-κB downstream inflammatory cytokines and chemokines, such as IL-1β, IL-6, TNF-α, intercellular adhesion molecule 1, monocyte chemo attractant protein 1 and iNOS, could also be suppressed (Lee et al., 2003; Speranza et al., 2012; Zheng et al., 2014). On the other hand, when the environment in the hippocampus improves, senescent cells might successfully resume normal cell-cycle progression and restore their original function (Van Deursen, 2014). Recently, research had linked the accumulation of senescent cells in aged tissues to a decline in health and a limit of lifespan. A growing list of studies indicated that the interventions that cleared senescent cells had achieved marked improvements in health span and lifespan (Yang and Sen, 2018). In our study, a significant reduction in senescent cells was observed in FASD rats after AST treatment. Furthermore, it was speculated that these senescent cells following AST treatment restored their function and prevented the spread of pro-inflammatory and pro-oxidative factors.

The role of nNOS expression in neurons treated with AST has not yet been revealed. This research tried to observe whether the nNOS of FASD rats has changed due to AST treatment. Interestingly, FASD rats treated with AST would increase nNOS expression in the hippocampal CA1 region. The increase in nNOS expression may be related to the recovery of senescent cells and there were several points about increased nNOS after AST treatment that could be considered: (1) neurons in the hippocampus had increased nNOS due to AST treatment, thus improving neuroprotection (Han et al., 2010); (2) Synaptic homeostasis mediated by nNOS made the connections between neurons in the hippocampus more stable (Joca et al., 2019), which was consistent with the greater distribution of ChAT+ fibers in the hippocampal CA1 region observed in this study; (3) NO catalyzed by nNOS could be used as a retrograde neurotransmitter to maintain glutamate exocytosis in the presynaptic terminal, leading to long-term potentiation (Picon-Pages et al., 2019). (4) NO catalyzed by nNOS activated heme-regulated eukaryotic initiation factor 2α kinase and further promoted dendritic spine growth (Picon-Pages et al., 2019).

AST treatment in FASD rats could help restore the cholinergic system in the MS nucleus and its axons projecting to the hippocampus, which is consistent with our previous report related to AD (Chen et al., 2021). Treatment of AST could restore the function of the ChAT+ neurons in the MS nucleus, caused by the expression of nerve growth factor (NGF), which could further prevent degeneration of cholinergic neurons (Nai et al., 2018). Furthermore, AST also restores brain-derived neurotrophic factor (BDNF) production in the cortex and hippocampus (Wu et al., 2014a, 2014b). Tyrosine kinase receptors activated by NGF and BDNF could increase the release of acetylcholine in synaptosomes (Knipper et al., 1994) and could increase the expression of nNOS in postsynaptic neurons (Tsumoto and Kohara, 2001).

The hippocampal CA1 pyramidal neurons in FASD rats after AST treatment significantly restored the densities of dendritic spines by 18–28%. Up-regulation of BDNF was also beneficial to dendritic spine

genesis; it could activate a protein kinase pathway, promoting neural formation, regeneration, and plasticity (Galasso et al., 2018). On the other hand, microglia might play another important role in the formation, modification, and elimination of synaptic structures (Wong et al., 2017). In this process, microglial process displayed end-feet morphological specializations and contacted a dendritic spine and an axon terminal, contributing to local remodeling during episodes of plasticity, including remodeling of dendritic spine and phagocytosis of the pre- and postsynaptic elements (Delpech et al., 2015; Tremblay and Majewska, 2011).

It was precisely because that AST had the ability to counteract oxidative stress and inflammatory response, where the hippocampal environment improved and the cholinergic system stabilized, then the pyramidal neurons in the hippocampal CA1 region could recover their synaptic structure and functions. Therefore, AST has great potential to improve the cognitive impairment of FASD. Since current data could only discuss the improvement effect of the FASD rat model after 8 days of AST treatment, it was not known whether it was still helpful for FASD animals after drug withdrawal. In the future, AST treatment in FASD may involve a single dose or require lifelong therapy to improve developmental and cognitive deficits after prenatal alcohol exposure, which will warrant further study.

Funding

This work was funded by the Ministry of Science and Technology of Taiwan to Chen, JR (MOST 109-2313-B-005-016).

CRediT authorship contribution statement

Mu-Hsuan Chen: Conceptualization; Methodology; Validation; Investigation; Data curation; Writing – original draft; Visualization. **Cih-Li Hong:** Methodology; Validation; Investigation; Visualization. **Yi-Ting Wang:** Methodology; Investigation. **Tsyr-Jiuan Wang:** Methodology; Resources; Writing - Review & Editing. **Jeng-Rung Chen:** Methodology; Resources; Writing – review & editing; Supervision; Project administration; Funding acquisition.

Conflict of interest

All authors declare no conflict of interest with the organizations that sponsored the research.

Acknowledgements

Mu-Hsuan Chen carried out his thesis research under the auspices of the Ph.D. Program in Tissue Engineering and Regenerative Medicine, National Chung-Hsing University and National Health Research institutes.

References

Aglawe, M.M., Kale, M.B., Rahangdale, S.R., Kotagale, N.R., Umekar, M.J., Taksande, B. G., 2021. Agmatine improves the behavioral and cognitive impairments associated with chronic gestational ethanol exposure in rats. Brain Res. Bull. 167, 37–47. https://doi.org/10.1016/j.brainresbull.2020.11.015.

Anthony, B., Vinci-Booher, S., Wetherill, L., Ward, R., Goodlett, C., Zhou, F.C., 2010. Alcohol-induced facial dysmorphology in C57BL/6 mouse models of fetal alcohol spectrum disorder. Alcohol 44 (7–8), 659–671. https://doi.org/10.1016/j.alcohol.2010.04.002.

Blanco, A.M., Pascual, M., Valles, S.L., Guerri, C., 2004. Ethanol-induced iNOS and COX-2 expression in cultured astrocytes via NF-kappa B. Neuroreport 15 (4), 681–685. https://doi.org/10.1097/00001756-200403220-00021.

Bogdan, C., 2001. Nitric oxide and the immune response. Nature 2 (10), 907–916. https://doi.org/10.1038/ni1001-907.

Brocardo, P.S., Gil-Mohapel, J., Christie, B.R., 2011. The role of oxidative stress in fetal alcohol spectrum disorders. Brain Res. Rev. 67 (1–2), 209–225. https://doi.org/10.1016/j.brainresrev.2011.02.001.

Charriaut-Marlangue, C., Bonnin, P., Pham, H., Loron, G., Leger, P.L., Gressens, P., Renolleau, S., Baud, O., 2013. Nitric oxide signaling in the brain: a new target for inhaled nitric oxide? Ann. Neurol. 73 (4), 442–448. https://doi.org/10.1002/ana.23842.

Chen, J.R., Lim, S.H., Chung, S.C., Lee, Y.F., Wang, Y.J., Tseng, G.F., Wang, T.J., 2017. Reproductive experience modified dendritic spines on cortical pyramidal neurons to enhance sensory perception and spatial learning in rats. Exp. Anim. 66 (1), 61–74. https://doi.org/10.1538/expanim.16-0061.

Chen, J.R., Tseng, G.F., Wang, Y.J., Wang, T.J., 2014. Exogenous dehydroisoandrosterone sulfate reverses the dendritic changes of the central neurons in aging male rats. Exp. Gerontol. 57, 191–202. https://doi.org/10.1016/j.exger.2014.06.010.

Chen, M.H., Wang, T.J., Chen, L.J., Jiang, M.Y., Wang, Y.J., Tseng, G.F., Chen, J.R., 2021. The effects of astaxanthin treatment on a rat model of Alzheimer's disease. Brain Res. Bull. 172, 151–163. https://doi.org/10.1016/j.brainresbull.2021.04.020.

Combs, C.K., Karlo, J.C., Kao, S.C., Landreth, G.E., 2001. beta-Amyloid stimulation of microglia and monocytes results in TNFalpha-dependent expression of inducible nitric oxide synthase and neuronal apoptosis. J. Neurosci. 21 (4), 1179–1188. https://doi.org/10.1523/jneurosci.21-04-01179.2001.

Delpech, J.C., Madore, C., Nadjar, A., Joffre, C., Wohleb, E.S., Laye, S., 2015. Microglia in neuronal plasticity: influence of stress. Neuropharmacology 96, 19–28. https://doi.org/10.1016/j.neuropharm.2014.12.034.

Deng, X.S., Deitrich, R.A., 2007. Ethanol metabolism and effects: nitric oxide and its interaction. Curr. Clin. Pharmacol. 2 (2), 145–153. https://doi.org/10.2174/157488407780598135.

Dobbing, J., Sands, J., 1979. Comparative aspects of the brain growth spurt. Early Hum. Dev. 3 (1), 79–83 https://doi.org/Doi 10.1016/0378-3782(79)90022-7.

Elibol-Can, B., Kilic, E., Yuruker, S., Jakubowska-Dogru, E., 2014. Investigation into the effects of prenatal alcohol exposure on postnatal spine development and expression of synaptophysin and PSD95 in rat hippocampus. Int. J. Dev. Neurosci. 33, 106–114. https://doi.org/10.1016/j.ijdevneu.2013.12.003.

Feng, Q., Ma, Y., Mu, S., Wu, J., Chen, S., Ouyang, L., Lei, W., 2014. Specific reactions of different striatal neuron types in morphology induced by quinolinic acid in rats. PLoS One 9, e91512. https://doi.org/10.1371/journal.pone.0091512.

Frechette, M., Rennie, K., Pappas, B.A., 2009. Developmental forebrain cholinergic lesion and environmental enrichment: behaviour, CA1 cytoarchitecture and neurogenesis. Brain Res. 1252, 172–182. https://doi.org/10.1016/j.brainres.2008.11.082.

Galasso, C., Orefice, I., Pellone, P., Cirino, P., Miele, R., Ianora, A., Brunet, C., Sansone, C., 2018. On the neuroprotective role of astaxanthin: new perspectives? Mar. Drugs 16 (8) https://doi.org/DOI: 10.3390/md16080247.

Garrett, J.E., Kim, I., Wilson, R.E., Wellman, C.L., 2006. Effect of N-methyl-d-aspartate receptor blockade on plasticity of frontal cortex after cholinergic deafferentation in rat. Neuroscience 140 (1), 57–66. https://doi.org/10.1016/j.neuroscience.2006.01.029.

Gil-Mohapel, J., Boehme, F., Kainer, L., Christie, B.R., 2010. Hippocampal cell loss and neurogenesis after fetal alcohol exposure: insights from different rodent models. Brain Res. Rev. 64 (2), 283–303. https://doi.org/10.1016/j.brainresrev.2010.04.011.

Guerin, M., Huntley, M.E., Olaizola, M., 2003. Haematococcus astaxanthin: applications for human health and nutrition. Trends Biotechnol. 21 (5), 210–216. https://doi.org/10.1016/S0167-7799(03)00078-7.

Han, S., Rudd, J.A., Hu, Z.Y., Zhang, L.H., Yew, D.T., Fang, M.R., 2010. Analysis of neuronal nitric oxide synthase expression and increasing astrogliosis in the brain of senescence-accelerated-prone 8 mice. Int. J. Neurosci. 120 (9), 602–608. https://doi.org/10.3109/00207454.2010.503911.

Hatano, E., Bennett, B.L., Manning, A.M., Qian, T., Lemasters, J.J., Brenner, D.A., 2001. NF-kappaB stimulates inducible nitric oxide synthase to protect mouse hepatocytes from TNF-alpha- and Fas-mediated apoptosis. Gastroenterology 120 (5), 1251–1262. https://doi.org/10.1053/gast.2001.23239.

Hen-Herbst, L., Jirikowic, T., Hsu, L.Y., Mccoy, S.W., 2020. Motor performance and sensory processing behaviors among children with fetal alcohol spectrum disorders compared to children with developmental coordination disorders. Res. Dev. Disabil. 103 https://doi.org/DOI: 10.1016/j.ridd.2020.103680.

Ito, Y., Hoare, M., Narita, M., 2017. Spatial and temporal control of senescence. Trends Cell Biol. 27 (11), 830–842. https://doi.org/10.1016/j.tcb.2017.07.004.

Joca, S.R.L., Sartim, A.G., Roncalho, A.L., Diniz, C.F.A., Wegener, G., 2019. Nitric oxide signalling and antidepressant action revisited. Cell Tissue Res. 377 (1), 45–58. https://doi.org/10.1007/s00441-018-02987-4.

Kane, C.J.M., Drew, P.D., 2021. Neuroinflammatory contribution of microglia and astrocytes in fetal alcohol spectrum disorders. J. Neurosci. Res. 99 (8), 1973–1985. https://doi.org/10.1002/jnr.24735.

Kanju, P.M., Parameshwaran, K., Sims-Robinson, C., Uthayathas, S., Josephson, E.M., Rajakumar, N., Dhanasekaran, M., Suppiramaniam, V., 2012. Selective cholinergic depletion in medial septum leads to impaired long term potentiation and glutamatergic synaptic currents in the hippocampus. PLoS One 7 (2) https://doi.org/DOI: 10.1371/journal.pone.0031073.

Karacay, B., Bonthius, N.E., Plume, J., Bonthius, D.J., 2015. Genetic absence of nNOS worsens fetal alcohol effects in mice. I: behavioral deficits. Alcohol Clin. Exp. Res. 39 (2), 212–220. https://doi.org/10.1111/acer.12616.

Knipper, M., Berzaghi, M.D., Blochl, A., Breer, H., Thoenen, H., Lindholm, D., 1994. Positive feedback between acetylcholine and the neurotrophins nerve growth-factor and brain-derived neurotrophic factor in the rat hippocampus. Eur. J. Neurosci. 6 (4), 668–671 https://doi.org/DOI 10.1111/j.1460-9568.1994.tb00312.x.

Lee, S.J., Bai, S.K., Lee, K.S., Namkoong, S., Na, H.J., Ha, K.S., Han, J.A., Yim, S.V., Chang, K., Kwon, Y.G., et al., 2003. Astaxanthin inhibits nitric oxide production and inflammatory gene expression by suppressing I kappa B kinase-dependent NF-kappa B activation. Mol. Cells 16 (1), 97–105.

Li, Z.R., Dong, X., Liu, H.L., Chen, X., Shi, H.Q., Fan, Y.S., Hou, D.S., Zhang, X.M., 2013. Astaxanthin protects ARPE-19 cells from oxidative stress via upregulation of Nrf2-regulated phase II enzymes through activation of PI3K/Akt. Mol. Vis. 19, 1656–1666.

Luo, J., 2015. Effects of ethanol on the cerebellum: advances and prospects. Cerebellum 14 (4), 383–385. https://doi.org/10.1007/s12311-015-0674-8.

Mandolesi, L., De Bartolo, P., Foti, F., Gelfo, F., Federico, F., Leggio, M.G., Petrosini, L., 2008. Environmental enrichment provides a cognitive reserve to be spent in the case of brain lesion. J. Alzheimers Dis. 15 (1), 11–28. https://doi.org/10.3233/jad-2008-15102.

McDermott, C.M., Hardy, M.N., Bazan, N.G., Magee, J.C., 2006. Sleep deprivation-induced alterations in excitatory synaptic transmission in the CA1 region of the rat hippocampus. J. Physiol. -Lond. 570 (3), 553–565. https://doi.org/10.1113/jphysiol.2005.093781.

Mooney, S.M., Napper, R.M.A., West, J.R., 1996. Long-term effect of postnatal alcohol exposure on the number of cells in the neocortex of the rat: a stereological study. Alcohol Clin. Exp. Res. 20 (4), 615–623 https://doi.org/DOI 10.1111/j.1530-0277.1996.tb01663.x.

Moser, M.B., Trommald, M., Andersen, P., 1994. An increase in dendritic spine density on hippocampal Ca1 pyramidal cells following spatial-learning in adult-rats suggests the formation of new synapses. P. Natl. Acad. Sci. USA 91 (26), 12673–12675 https://doi.org/DOI 10.1073/pnas.91.26.12673.

Nacarelli, T., Lau, L., Fukumoto, T., Zundell, J., Fatkhutdinov, N., Wu, S., Aird, K.M., Iwasaki, O., Kossenkov, A.V., Schultz, D., et al., 2019. NAD+ metabolism governs the proinflammatory senescence-associated secretome. Nat. Cell Biol. 21 (3), 397–407. https://doi.org/10.1038/s41556-019-0287-4.

Nai, Y., Liu, H., Bi, X.Z., Gao, H.Y., Ren, C., 2018. Protective effect of astaxanthin on acute cerebral infarction in rats. Hum. Exp. Toxicol. 37 (9), 929–936. https://doi.org/10.1177/0960327117745693.

Norman, A.L., Crocker, N., Mattson, S.N., Riley, E.P., 2009. Neuroimaging and fetal alcohol spectrum disorders. Dev. Disabil. Res. Rev. 15 (3), 209–217. https://doi.org/10.1002/ddrr.72.

Nunez, S.C., Roussotte, F., Sowell, E.R., 2011. Focus on: structural and functional brain abnormalities in fetal alcohol spectrum disorders. Alcohol Res. Health 34 (1), 121–131.

Ohkawa, H., Ohishi, N., Yagi, K., 1979. Assay for lipid peroxides in animal tissues by thiobarbituric acid reaction. Anal. Biochem. 95 (2), 351–358. https://doi.org/10.1016/0003-2697(79)90738-3.

Patten, A.R., Fontaine, C.J., Christie, B.R., 2014. A comparison of the different animal models of fetal alcohol spectrum disorders and their use in studying complex behaviors. Front. Pediatr. 2 https://doi.org/DOI: 10.3389/fped.2014.00093.

Petrelli, B., Weinberg, J., Hicks, G.G., 2018. Effects of prenatal alcohol exposure (PAE): insights into FASD using mouse models of PAE. Biochem. Cell Biol. 96 (2), 131–147. https://doi.org/10.1139/bcb-2017-0280.

Picon-Pages, P., Garcia-Buendia, J., Munoz, F.J., 2019. Functions and dysfunctions of nitric oxide in brain. Bba-Mol. Basis Dis. 1865 (8), 1949–1967. https://doi.org/10.1016/j.bbadis.2018.11.007.

Piechota, M., Sunderland, P., Wysocka, A., Nalberczak, M., Sliwinska, M.A., Radwanska, K., Sikora, E., 2016. Is senescence-associated β-galactosidase a marker of neuronal senescence? Oncotarget 7 (49), 81099–81109. https://doi.org/10.18632/oncotarget.12752.

Qin, L.Y., Crews, F.T., 2012. NADPH oxidase and reactive oxygen species contribute to alcohol-induced microglial activation and neurodegeneration. J. Neuroinflamm. 9 https://doi.org/DOI: 10.1186/1742-2094-9-5.

Robertson, R.T., Gallardo, K.A., Claytor, K., Ha, D.H., Ku, K.H., Yu, B.P., Lauterborn, J.C., Wiley, R.G., Yu, J., Gall, C.M., et al., 1998. Neonatal treatment with 192 IgG-saporin produces long-term forebrain cholinergic deficits and reduces dendritic branching and spine density of neocortical pyramidal neurons. Cereb. Cortex 8 (2), 142–155 https://doi.org/DOI 10.1093/cercor/8.2.142.

Shabab, T., Khanabdali, R., Moghadamtousi, S.Z., Kadir, H.A., Mohan, G., 2017. Neuroinflammation pathways: a general review. Int. J. Neurosci. 127 (7), 624–633. https://doi.org/10.1080/00207454.2016.1212854.

Shen, H., Kuo, C.C., Chou, J., Delvolve, A., Jackson, S.N., Post, J., Woods, A.S., Hoffer, B. J., Wang, Y., Harvey, B.K., 2009. Astaxanthin reduces ischemic brain injury in adult rats. Faseb J. 23 (6), 1958–1968. https://doi.org/10.1096/fj.08-123281.

Sikora, E., Bielak-Zmijewska, A., Dudkowska, M., Krzystyniak, A., Mosieniak, G., Wesierska, M., Wlodarczyk, J., 2021. Cellular senescence in brain aging. Front. Aging Neurosci. 13. https://doi.org/10.3389/fnagi.2021.646924.

Speranza, L., Pesce, M., Patruno, A., Franceschelli, S., de Lutiis, M.A., Grilli, A., Felaco, M., 2012. Astaxanthin treatment reduced oxidative induced pro-inflammatory cytokines secretion in U937: SHP-1 as a novel biological target. Mar. Drugs 10 (4), 890–899. https://doi.org/10.3390/md10040890.

Swanson, D.J., Tonjes, L., King, M.A., Walker, D.W., Heaton, M.B., 1996. Influence of chronic prenatal ethanol on cholinergic neurons of the septohippocampal system. J. Comp. Neurol. 364 (1), 104–112 https://doi.org/Doi 10.1002/(Sici)1096-9861(19960101)364:1<104::Aid-Cne9>3.0.Co;2-9.

Topper, L.A., Baculis, B.C., Valenzuela, C.F., 2015. Exposure of neonatal rats to alcohol has differential effects on neuroinflammation and neuronal survival in the cerebellum and hippocampus. J. Neuroinflamm. 12 https://doi.org/DOI: 10.1186/s12974-015-0382-9.

Tremblay, M., Majewska, A.K., 2011. A role for microglia in synaptic plasticity? Commun. Integr. Biol. 4 (2), 220–222. https://doi.org/10.4161/cib.4.2.14506.

Tsumoto, T., Kohara, K., 2001. Response: BDNF as an anterophin; a novel neurotrophic relationship between brain neurons. Trends Neurosci. 24 (12), 684–685 https://doi.org/Doi 10.1016/S0166-2236(00)01983-4.

Van Deursen, J.M., 2014. The role of senescent cells in ageing. Nature 509 (7501), 439–446. https://doi.org/10.1038/nature13193.

Wang, J.Y., Lee, Y.J., Chou, M.C., Chang, R., Chiu, C.H., Liang, Y.J., Wu, L.S., 2015. Astaxanthin protects steroidogenesis from hydrogen peroxide-induced oxidative stress in mouse leydig cells. Mar. Drugs 13 (3), 1375–1388. https://doi.org/10.3390/md13031375.

Wang, Y., Liu, Y., Li, Y., Liu, B., Wu, P., Xu, S., Shi, H., 2019. Protective effects of astaxanthin on subarachnoid hemorrhage-induced early brain injury: Reduction of cerebral vasospasm and improvement of neuron survival and mitochondrial function. Acta Histochem. 121 (1), 56–63. https://doi.org/10.1016/j.acthis.2018.10.014.

Watson, R.E., Desesso, J.M., Hurtt, M.E., Cappon, G.D., 2006. Postnatal growth and morphological development of the brain: a species comparison. Birth Defects Res. B Dev. Reprod. Toxicol. 77 (5), 471–484. https://doi.org/10.1002/bdrb.20090.

Wattendorf, D.J., Muenke, M., 2005. Fetal alcohol spectrum disorders. Am. Fam. Physician 72 (2), 279–282, 285.

White, A.M., Matthews, D.B., Best, P.J., 2000. Ethanol, memory, and hippocampal function: a review of recent findings. Hippocampus 10 (1), 88–93. https://doi.org/10.1002/(sici)1098-1063(2000)10:1<88::Aid-hipo10>3.0.Co;2-l.

Wilhoit, L.F., Scott, D.A., Simecka, B.A., 2017. Fetal alcohol spectrum disorders: characteristics, complications, and treatment. Community Ment. Hlt. J. 53 (6), 711–718. https://doi.org/10.1007/s10597-017-0104-0.

Wong, E.L., Stowell, R.D., Majewska, A.K., 2017. What the spectrum of microglial functions can teach us about fetal alcohol spectrum disorder. Front. Synaptic Neurosci. 9, 11. https://doi.org/10.3389/fnsyn.2017.00011.

Wu, H.J., Niu, H.J., Shao, A.W., Wu, C., Dixon, B.J., Zhang, J.M., Yang, S.X., Wang, Y.R., 2015. Astaxanthin as a potential neuroprotective agent for neurological diseases. Mar. Drugs 13 (9), 5750–5766. https://doi.org/10.3390/md13095750.

Wu, Q., Zhang, X.S., Wang, H.D., Zhang, X., Yu, Q., Li, W., Zhou, M.L., Wang, X.L., 2014. Astaxanthin activates nuclear factor erythroid-related factor 2 and the antioxidant responsive element (Nrf2-ARE) pathway in the brain after subarachnoid hemorrhage in rats and attenuates early brain injury. Mar. Drugs 12 (12), 6125–6141. https://doi.org/10.3390/md12126125.

Wu, W.Q., Wang, X., Xiang, Q.S., Meng, X., Peng, Y., Du, N., Liu, Z.G., Sun, Q.C., Wang, C., Liu, X.B., 2014. Astaxanthin alleviates brain aging in rats by attenuating oxidative stress and increasing BDNF levels. Food Funct. 5 (1), 158–166. https://doi.org/10.1039/c3fo60400d.

Yang, N., Sen, P., 2018. The senescent cell epigenome. Aging 10 (11), 3590–3609. https://doi.org/10.18632/aging.101617.

Yeh, P.T., Huang, H.W., Yang, C.M., Yang, W.S., Yang, C.H., 2016. Astaxanthin inhibits expression of retinal oxidative stress and inflammatory mediators in streptozotocin-induced diabetic rats. PLoS One 11 (1). https://doi.org/10.1371/journal.pone.0146438.

Zhang, Y.P., Wang, H.X., Li, Y., Peng, Y., 2018. A review of interventions against fetal alcohol spectrum disorder targeting oxidative stress. Int. J. Dev. Neurosci. 71, 140–145. https://doi.org/10.1016/j.ijdevneu.2018.09.001.

Zheng, D., Li, Y., He, L., Tang, Y.M., Li, X.P., Shen, Q.Y., Yin, D.L., Peng, Y., 2014. The protective effect of astaxanthin on fetal alcohol spectrum disorder in mice. Neuropharmacology 84, 13–18. https://doi.org/10.1016/j.neuropharm.2014.04.013.